Available online at www.sciencedirect.com
SCIENCE DIRECT
Lithos 89 (2006) 275–299
LITHOS
www.elsevier.com/locate/lithos

Mineral phase compositions in silica-undersaturated 'leucite' lamproites from the Bucak area, Isparta, SW Turkey

Hakan Çoban [a,*], Martin F.J. Flower [b]

[a] Geology Department, Engineering and Architecture Faculty, Suleyman Demirel University, 32260, Isparta, Turkey
[b] Department of Earth and Environmental Sciences (M/C 186), University of Illinois at Chicago, Illinois 60607-7059, USA

Received 11 August 2004; accepted 23 December 2005
Available online 17 February 2006

Abstract

Ultrapotassic rocks in the Bucak area of Isparta Angle, SW Turkey, show unusually low SiO_2 (46.8–49.2 wt.%) and high MgO (10.4–11.6 wt.%) contents, and lamproitic affinity (K/Na, >2.5; Mg#, 73–75; Al_2O_3, 9.2–11 wt.%, CaO 7.4–10.6 wt.%, Cr, 525–675 ppm; Ni, 442–615 ppm). They are made up by phlogopite (30–40 vol.%), leucite (25–30 vol.%), olivine (5–20 vol.%), which rarely contain Cr-spinel, clinopyroxene (5–10 vol.%), sanidine (5 vol.%) and richterite, with accessory apatite, magnetite and ilmenite. One sample also include negligible sodalite in groundmass, which is unusual mineral in lamproites. Mineral phase variation and textures record discrete phases of pre-eruptive crystallization: (1) early appearance of (Cr-spinel-bearing) olivine, Ti poor phlogopite ± apatite at pressures of ca. 1.0–2.0 GPa, at or close to the lithospheric Mechanical Boundary Layer (MBL), and (2) later appearance of Ti rich phlogopite, clinopyroxene, richterite, leucite, sanidine, and other minor phases, at pressures of ca. 0.1–1.0 GPa, indicating discrete, pressure-specific fractionation events. The Bucak silica poor 'leucite' lamproites were probably generated by partial melting of phlogopite-bearing, refractory peridotite at pressures of ca. 1.5–2 GPa, higher than those proposed for SiO_2-saturated 'phlogopite' lamproites (ca. 1–1.5 GPa) from Afyon, to the North. The depth (total pressure) of melt segregation probably dominates over volatile partial pressures (e.g. of CO_2, F, H_2O) in determining the SiO_2-undersaturated character of Bucak magmas.

Keywords: Silica undersaturation; Lamproite; Mineral chemistry; Bucak; Isparta; SW Turkey

1. Introduction

Ultrapotassic (peralkaline to lamproitic) magmatic activity affected SW Turkey in several regions between ca. 14.8 Ma and 4.6 Ma, e.g. Afyon-Sandikli (Besang et al., 1977; Keller, 1983; Aydar et al., 1995, 1996; Aydar, 1998; Savascin and Oyman, 1998; Francalanci et al., 1990, 2000; Akal and Helvaci, 2002), Bodrum (Pe and Gledhill, 1975; Gulec, 1991; Robert et al., 1992), Denizli (Ercan et al., 1983, 1985, 1996; Savascin and Gulec, 1990; Gulec, 1991; Paton, 1992), and Isparta-Bucak (Lefevre et al., 1983; Yagmurlu et al., 1997; Francalanci et al., 1990, 2000; Doglioni et al., 2002), marking the transition from subduction- to collision-related tectonic regimes (Fig. 1).

Plagioclase-rich ultrapotassic rocks from Bodrum and Denizli are relatively rich in Al_2O_3 (Robert et al., 1992; Ercan et al., 1983) while lamproites from Afyon-Sandikli comprise assemblages of phlogopite,

* Corresponding author. Tel.: +90 246 211 1331; fax: +90 246 237 0859.
E-mail address: coban@mmf.sdu.edu.tr (H. Çoban).

0024-4937/$ - see front matter © 2006 Elsevier B.V. All rights reserved.
doi:10.1016/j.lithos.2005.12.006

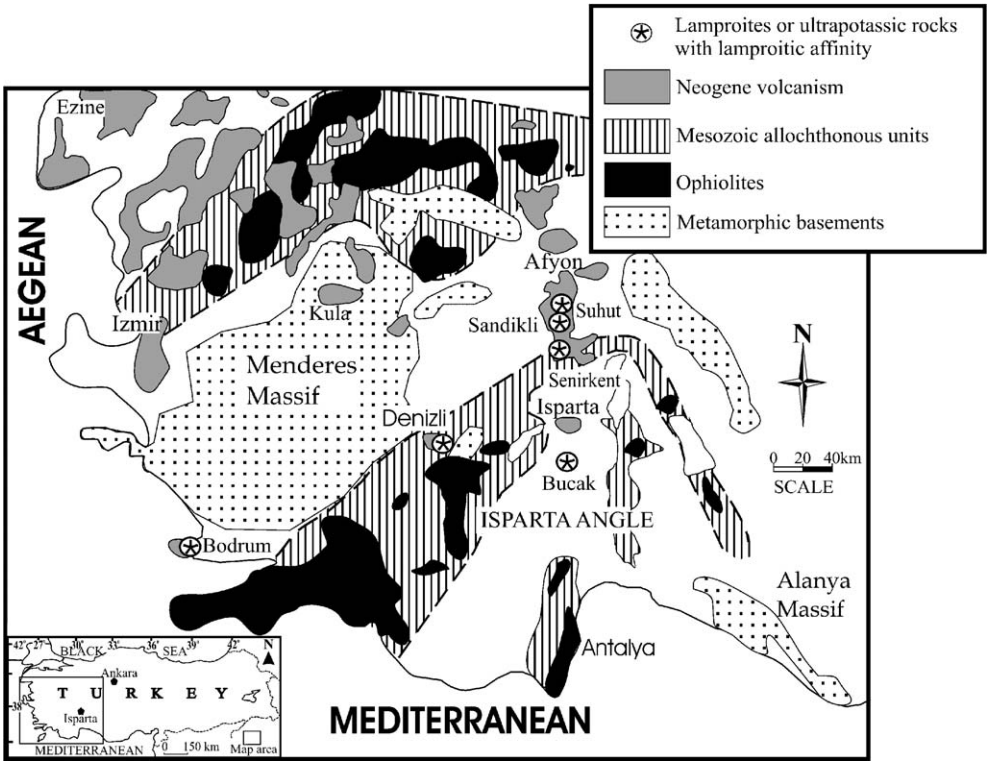

Fig. 1. Simplified map showing the distribution of metamorphic basement rocks, ophiolitic complexes, Neogene volcanics and lamproite occurrences from Western Anatolia. Data source: metamorphic basements from Bozkurt and Oberhansli (2001); ophiolites after Robertson (2002); Neogene volcanics modified from Ercan et al. (1996), and Isparta Angle lamproitic occurrences after Besang et al. (1977), Keller (1983), Aydar et al. (1995), Aydar (1998), Savascin and Oyman (1998), Ercan et al. (1983, 1985), Gulec (1991), Francalanci et al. (1990, 2000), Akal and Helvaci (2002) and Robert et al. (1992).

K-richterite, olivine, diopside, sanidine, apatite and calcite (Akal and Helvaci, 2002). In contrast, lamproites from the Bucak region are distinguished by their near-primary magmatic character, SiO_2 contents ranging 46.8–49.2 wt.%, and MgO, 10.4–11.6 wt.%. However, while their liquidus phase assemblages have not been characterized in detail (Lefevre et al., 1983; Yagmurlu et al., 1997; Francalanci et al., 1990, 2000), the available whole-rock data suggest that many of these ultrapotassic magmas tap refractory (i.e. basalt-depleted) mantle sources. In this paper, the first of two, we present electron microprobe data for the Bucak lamproitic mineral phases, significantly on the genetic conditions of these SiO_2-undersaturated magmas.

2. Geological setting

Bucak lamproites are exposed ca. 50 km south of Isparta within the tectonically complex 'Isparta Angle' region (Fig. 1). The Isparta Angle comprises several structural components—the Menderes Massive, Afyon 'metabasement' (including the Alanya massif) (Bozkurt and Oberhansli, 2001), Neo-Tethyan ophiolite fragments (including the Lycian, Antalya and Beyşehir-Hoyran nappes; Robertson, 2000, 2002), and the distinctive Afyon-Isparta Neogene volcanic province (Kocyigit, 1984; Aydar et al., 1995, 1996, 2003; Aydar, 1998; Yagmurlu et al., 1997; Doglioni et al., 2002) (Fig. 1). The appearance of potassic and ultrapotassic magmatic activity appears to have coincided with an episode of post-collision lithosphere extension and the initiation of strike-slip, transtensional faulting (Kocyigit, 1984; Savascin and Oyman, 1998; Aydar, 1998; Yagmurlu et al., 1997; Francalanci et al., 2000; Kocyigit et al., 2002; Doglioni et al., 2002; Aydar et al., 2003; Cihan et al., 2003; Gursoy et al., 2003; Vaughan and Scarrow, 2003). The volcanic activity appeared during the Late Miocene and Pliocene following sporadic calcalkaline activity in the Early Miocene, to be succeeded in the Quaternary by a short episode of alkali basalt eruptions (Aydar, 1998). Although the Isparta Angle lies more than 200 km north of both the Hellenic and

Cyprian subduction systems (Fig. 2), it appears to represent an extensional ('back-arc') response to northward African plate subduction (Kocyigit, 1984; Glover and Robertson, 1998a,b; Papazachos and Papaioannou, 1999; Doglioni et al., 2002). In general, igneous activity in the southern part of the Isparta Angle comprises two types: (1) SiO_2-saturated trachyte-trachyandesites, within and to the south of the Gölcük-Isparta region (Lefevre et al., 1983; Alici et al., 1998), and (2) SiO_2-undersaturated activity in the vicinity of Bucak (Lefevre et al., 1983; Francalanci et al., 2000), between 4.07±0.2 and 4.7±0.13 Ma (Lefevre et al., 1983) (Fig. 2). The latter penetrated Mesozoic and Tertiary sediments and Late Cretaceous ophiolite remnants (Hancer and Karaman, 2001) and is mostly preserved as small-volume dikes and lavas.

3. Petrography

Porphyric, gray-greenish Bucak rocks are made up by phlogopite (30–40 vol.%), leucite (25–30 vol.%), olivine (5–20 vol.%) (with rare Cr-spinels), clinopyroxene (5–10 vol.%), sanidine (5 vol.%), apatite, subsidiary amounts of richterite, Fe–Ti oxides and unidentified Ca–Ti niobates. One sample includes

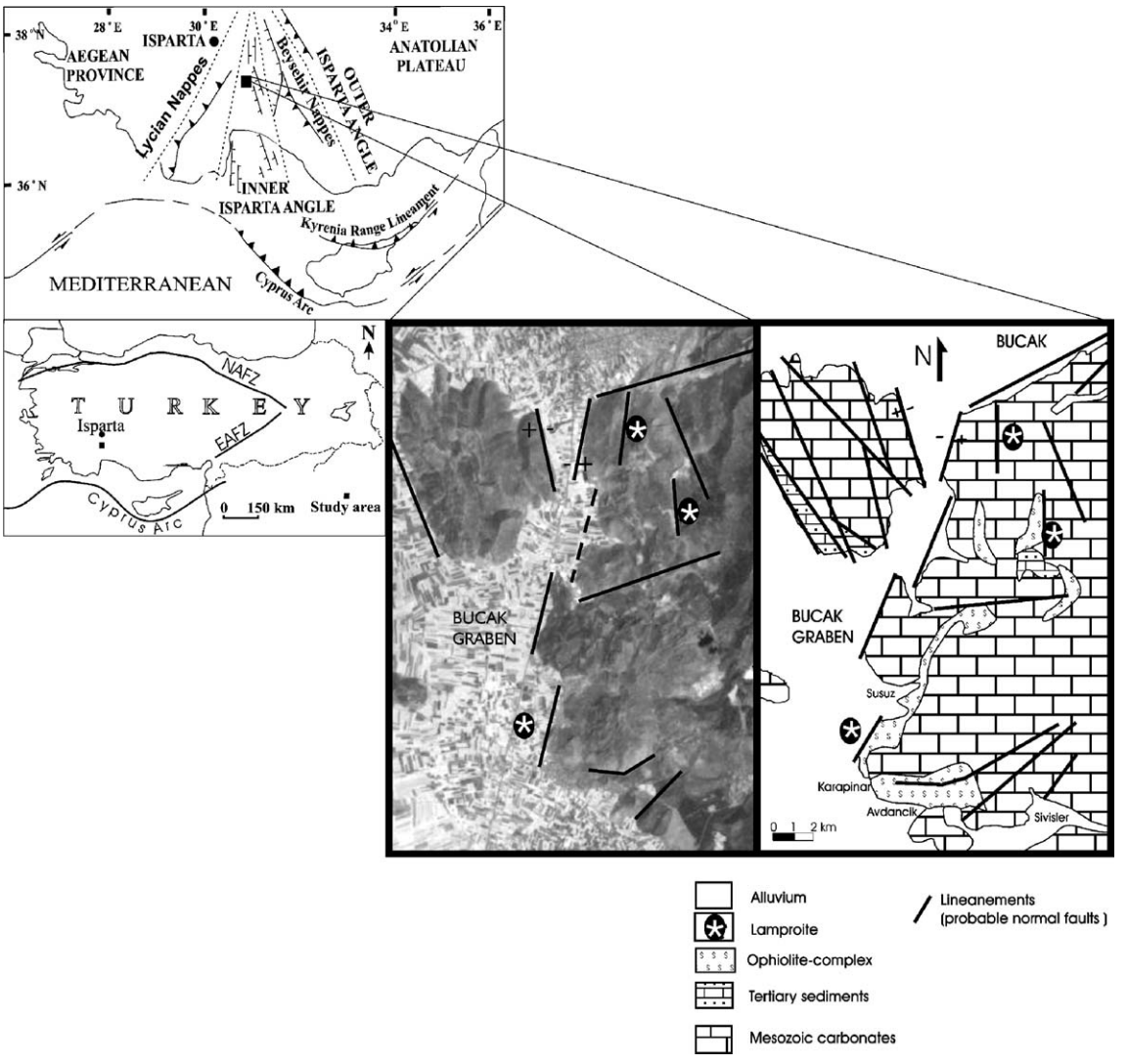

Fig. 2. Main Neotectonic lineaments and structural units of Isparta Angle (after Glover and Robertson, 1998b), and simplified geological map—landsad image of Bucak area. EAFZ: East Anatolian Fault Zone, NAFZ: North Anatolian Fault Zone.

negligible sodalite in groundmass, which is unusual mineral in lamproites. Phologopite present mostly as a groundmass phase, and to a lesser extent as an early formed phenocryst phase (Fig. 3a). Early formed phlogopite and olivine are the only phenocryst phases in the Bucak rocks. Olivine occurs in different forms as anhedral or subhedral hopper type, skeletal and polyhedral crystals (Fig. 4a), and scarcely rounded microphenocrysts in the groundmass, which are related to rapid growth of olivine in a cooling magma (Donaldson, 1976, 1979). The following textural relations were observed in Bucak rocks: Cr-spinel inclusions in olivine (Fig. 4b); olivine mantled by phlogopite, a typical feature of H_2O-rich ultra-potassic magmas (Arima and Edgar, 1983; Luth, 1967), and peritectic reaction is evidenced for phlogopite formation by reaction of olivine with potassic melt (Luth, 1967; Carmichael, 1967; Mitchell, 1981; Wagner and Velde, 1986; Conticelli et al., 1992) (Fig. 4a); apatite inclusions in groundmass phlogopite; richterite in the groundmass; formation of prismatic clinopyroxene microphenocrysts and rounded leucite by resorption (or breakdown) of phlogopite (Fig. 3b, c and d); leucite rimmed by groundmass sanidine (Fig.

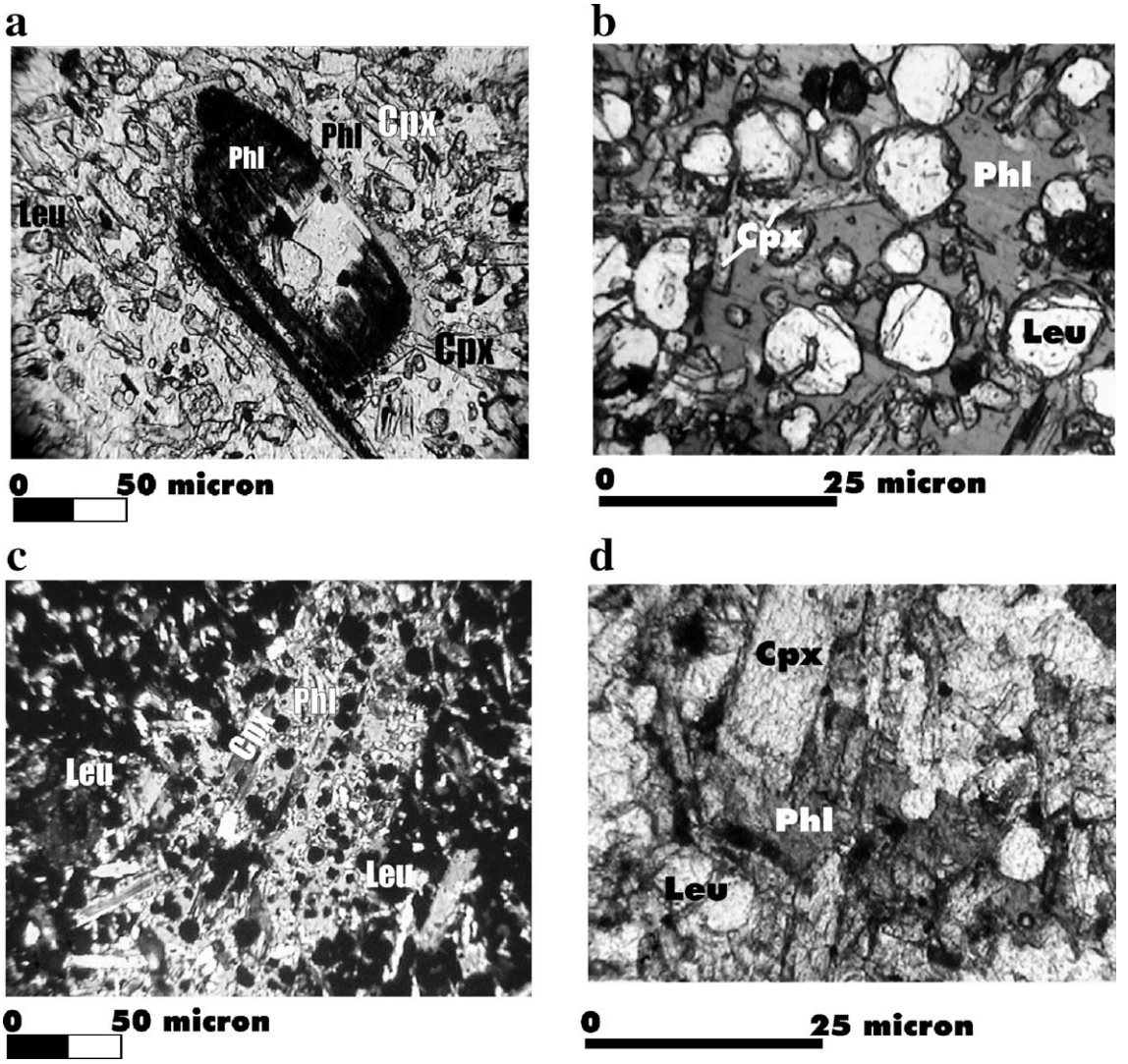

Fig. 3. (a) Mantled Type I phlogopite (phl) phenocryst (in centre) enclosed by resorbed groundmass (Type II) phlogopite and its resorption products (leucites—leu and clinopyroxenes—cpx). (b, c and d) The formation of rounded twin free leucite (leu) and prismatic clinopyroxenes (cpx) by resorption (or breakdown) of groundmass Type II phlogopite (phl).

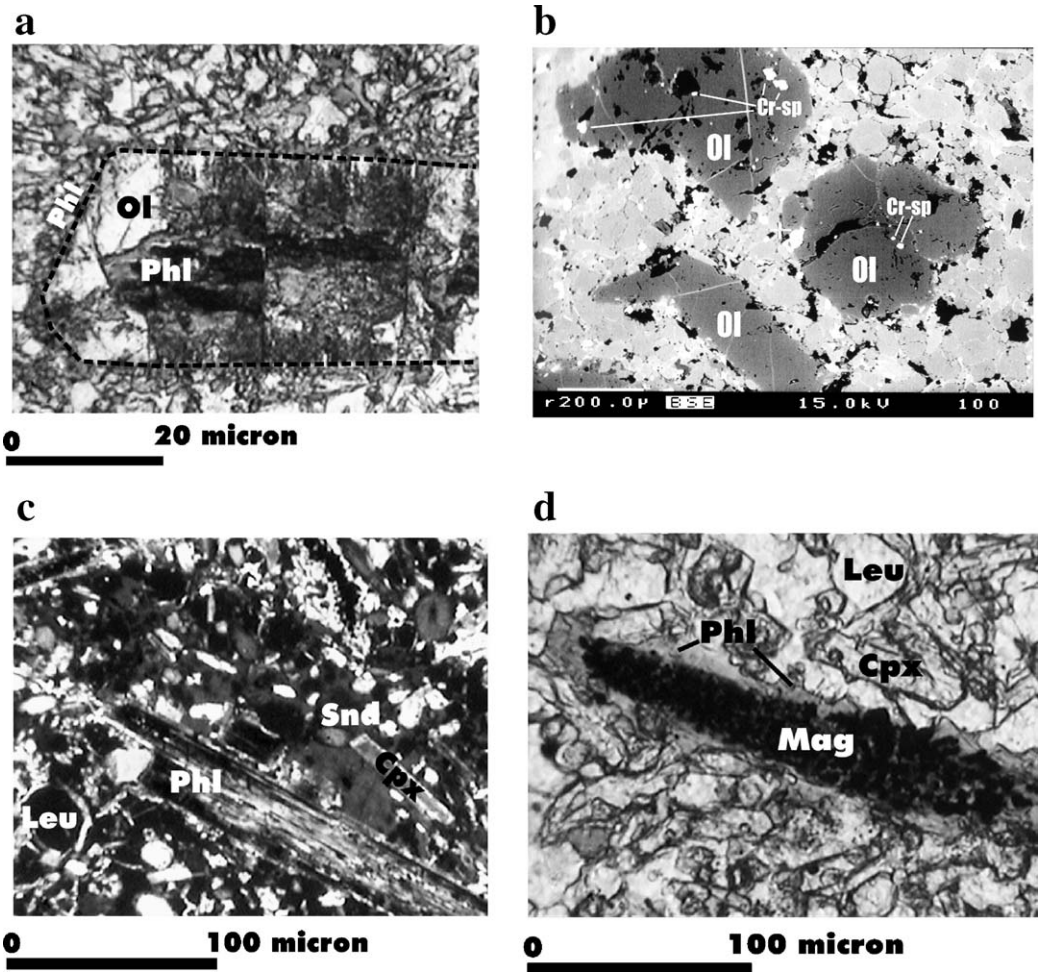

Fig. 4. (a) Skeletal olivine (ol) rimmed by phlogopite (phl) phenocrysts; (b) anhedral Cr-spinel (Cr-sp) inclusions in resorbed olivine phenocrysts; (c) the groundmass sanidine (Snd) as mesostas, and a reaction rim between leucite (leu) and sanidine indicating the sanidine inversion from leucite; (d) the formation of magnetite (Mag) by the breakdown of resorbed phlogopite, coexist with leucite and clinopyroxenes.

4c); formation of Fe–Ti oxides by breakdown of phlogopites (Fig. 4d). Following the appearance of Cr-rich spinel, the crystallization sequence is marked by; olivine, Type I phlogopite, and apatite, prior to Type II phlogopite, richterite, diopside, and leucite, which formed as a resorption product of the micas, and, eventually, groundmass sanidine, leucite, and Fe–Ti oxides.

4. Analytical methods

Major and trace element analyses of selected 8 unaltered rock samples were carried out at the University of Lausanne (Switzerland), using Philips PW 2400X-ray fluorescent spectrometer. Rare earth elements have been analyzed by ICPMS (inductively coupled plasma emission spectrometer). Detection limit and range for trace elements are 0.5 ppm and 0.007–0.012 ppm respectively. Accuracy and precision was evaluated by analyzing international reference samples AGV-1, BHV-0, MFTH, QLO, GSP, STM. Mineral compositions were determined using (1) a JEOL-5900 SEM-EDS electron microprobe (at Lakehead University, Canada) for which operating conditions were 15 kV and 20 nA, and (2) a CAMECA-SX-51 electron microprobe (at Heidelberg University, Germany) for which operating conditions were 15 kV and 20 nA, and counting time of usually 10 s. Electron beam size was 1 μm except when analyzing feldspar for which a 10 μm beam was required. Natural and synthetic oxide and silicate standards were used. Correction procedures were performed with CAMECAS' PAP software for on-line data reduction.

5. Whole-rock chemistry and classification

Analyzed rocks are phonotephrites, according to Le Maitre et al. (2002) classification, but whole-rock compositions define these rocks as ultrapotassic ($K_2O/Na_2O > 2.5$) in type (Table 1; Fig. 5a), with SiO_2 ranging between 46.80 and 49.19 wt.%, Al_2O_3 9.19–11 wt.%, CaO, 7.34–10.60 wt.% and MgO 10.39–11.64 wt.%. Ni contents range 442–615 ppm, Cr 525–675 ppm and Mg# ($Mg/Mg+Fe^{2+}$) 73–75 are consistent with near-primary magmas equilibrated with peridotitic mantle sources. The MgO-rich, Al_2O_3-poor character and extreme enrichment in Ba (1608–2528 ppm), Sr (1582–2290 ppm), F (6200–6900 ppm) and Zr (473–1026 ppm) are typical of lamproites (Foley et al., 1987; Mitchell and Bergman, 1991) and conform to Group I in the ultrapotassic classification scheme of Foley et al. (1987) (Fig. 5b). Although still lamproitic in character (i.e. showing $MgO > 3$ wt.%, $Al_2O_3 < 13$ wt.%, and $K_2O/Na_2O > 1.5$) other ultrapotassic rocks exposed in

Table 1
Representative major oxide (wt.%), trace element and REE (ppm) compositions of Bucak rocks

Sample no.	B3-TB-a	B5T-a	BT1-a	B-7T-a	B5T	B7T	B-1	B-2
Major								
SiO_2	48.45	47.18	47.83	48.86	49.19	47.98	48.90	46.80
TiO_2	1.99	1.51	1.71	1.72	1.77	1.64	1.75	1.70
Al_2O_3	10.63	9.69	9.19	10.37	10.82	11.00	10.30	10.80
Fe_2O_{3tot}	6.91	7.24	7.16	6.72	6.81	7.29	6.82	7.30
MnO	0.12	0.16	0.11	0.12	0.11	0.12	0.10	0.10
MgO	10.60	11.67	11.19	10.50	10.39	11.64	11.20	11.50
CaO	8.52	9.52	8.52	8.23	8.39	9.11	7.34	10.60
Na_2O	1.85	1.30	2.13	2.60	1.95	1.64	2.23	1.60
K_2O	6.05	6.84	6.57	6.74	6.32	4.81	7.40	5.80
P_2O_5	1.28	1.53	1.42	1.34	1.56	1.42	1.11	1.60
Cr_2O_3	0.09	0.11	0.08	0.08	0.09	0.08	0.11	0.09
NiO	0.06	0.08	0.07	0.06	0.06	0.07	0.09	0.06
L.O.I.	2.85	3.31	2.98	1.79	1.68	2.11	1.60	2.30
Total	99.39	100.14	99.04	99.15	99.11	99.13	99.10	100.25
Mg#	73.22	74.18	73.60	73.59	73.12	74.00	74.54	73.74
Trace								
Ba	2380	1971	2268	2302	2284	2528	1608	1983
Sr	1878	1595	1582	1928	1997	2290	1584	2103
Rb	525	236	367	268	604	338	293	328
Zr	960	1001	1026	929	990	882	616	473
Nb	166	200	203	161	173	146	184	146
Y	24	27	22	23	24	26	24	26
Th	24	22	21	22	24	16	16	16
Ta	10	9	10	8	10	6	8	10
Hf	20	19	19	18	19	18	23	17
REE								
La	160.32	132.56	132.65					
Ce	293.47	230.21	246.72					
Pr	31.16	24.58	26.40					
Nd	115.12	90.21	96.88					
Sm	16.08	13.42	13.91					
Eu	4.28	3.34	3.69					
Gd	10.72	9.11	9.72					
Tb	1.16	1.12	0.94					
Dy	5.24	5.70	4.79					
Ho	0.86	0.95	0.75					
Er	2.22	2.48	2.01					
Tm	0.24	0.31	0.25					
Yb	1.55	2.28	1.52					
Lu	0.23	0.31	0.26					

Mg# = atomic $100 * (Mg/Mg+Fe^{2+})$, assuming that $Fe^{3+}/\sum Fe = 0.85$.

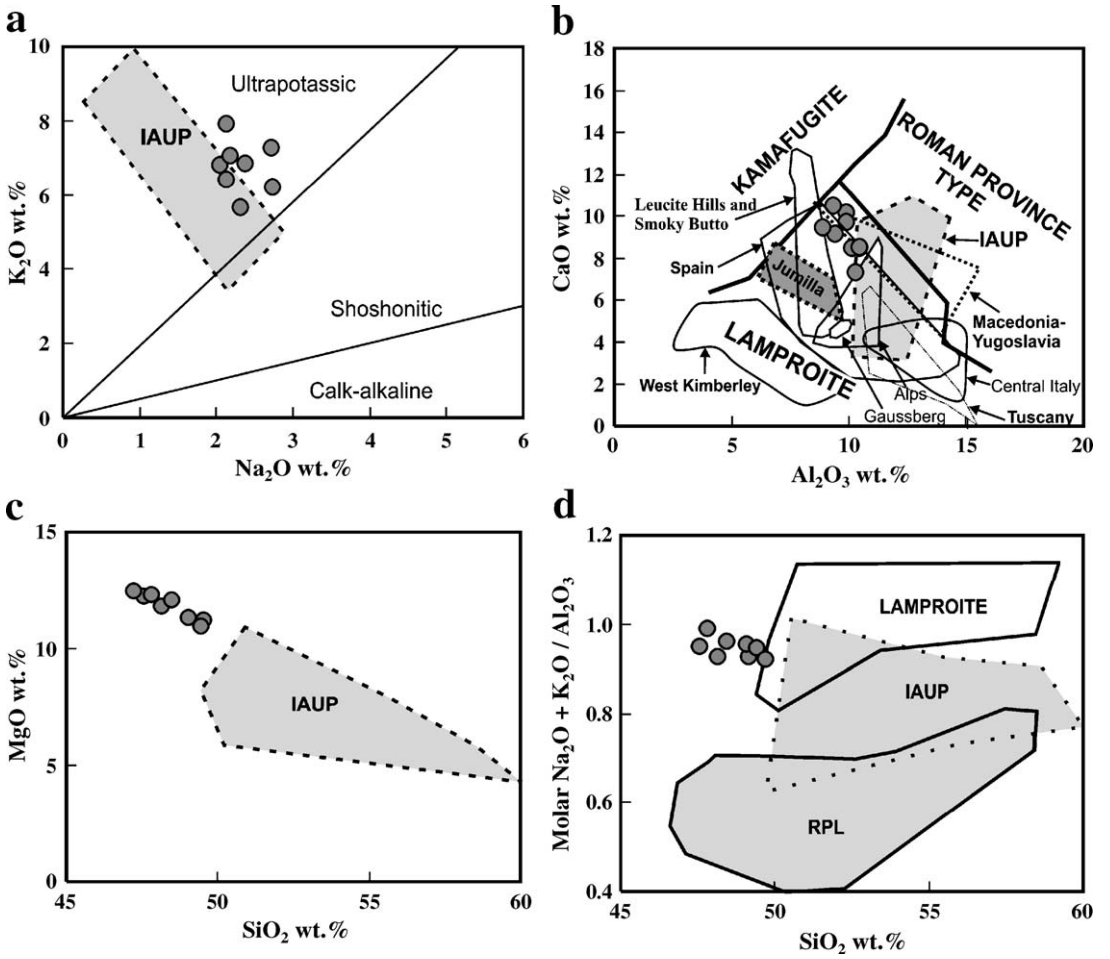

Fig. 5. Bucak ultrapotassic rocks (filled circle) plotted on (a) K_2O (wt.%) versus Na_2O (wt.%), (b) CaO (wt.%) versus Al_2O_3 (wt.%)—classification of ultrapotassic rocks (Foley et al., 1987) (fields from Tuscany lamproites after Conticelli et al., 1992 and other lamproite occurrences after Altherr et al., 2004; references therein), and (c) MgO (wt.%) versus SiO_2 (wt.%) and (d) K_2O+Na_2O/Al_2O_3 (molar) versus SiO_2 (wt.%) diagrams. For comparison data also include other Isparta Angle ultrapotassic rocks (IAUP—dashed line) having lamproitic affinity (assuming MgO > 3 wt.%, Al_2O_3 < 13 wt.% and K_2O/Na_2O > 1.5), after Besang et al. (1977), Keller (1983), Ercan et al. (1983, 1985), Gulec (1991), Robert et al. (1992), Aydar et al. (1996) and Akal and Helvaci (2002). RPL and lamproite fields on diagram 'd' after Bergman (1987) and Mitchell and Bergman (1991).

the Isparta Angle (referred to as IAUP) (e.g. Bodrum, Denizli and Afyon-Sandikli) appear to be transitional to 'Roman' shoshonitic types (Fig. 5a, b and d). However, the Bucak compositions differ significantly from these, showing lower SiO_2 and higher MgO, Cr, Ni contents, suggesting they represent near-primary magmas (Fig. 5c).

Compared to other reported silica-poor ultrapotassic rocks with lamproitic affinity from the Mediterranean region (e.g. Jumilla, SE Spain, Venturelli et al., 1991 and Macedonia–Yugoslavia, East European, Cvetkovic' et al., 2004; Altherr et al., 2004), the Bucak lavas show low Th (16–24 ppm), and high Ta (6–10 ppm), Nb (160–200 ppm) and REE contents, the latter being strongly fractionated (Ce/Nd, 2.4–2.5, cf. 1.51–1.74 in Mediterranean types, Foley et al., 1987) and lacking negative Eu anomalies (Fig. 6a and b). Their relatively high P_2O_5 (1.1–1.62 wt.%) contents resemble those of lamproites from Jumilla, Spain (1.55–2.26 wt.%; Venturelli et al., 1991) and from Macedonia–Yugoslavia, East European (up to 1.73 wt.%; Cvetkovic' et al., 2004; Altherr et al., 2004).

In general, SiO_2-undersaturated lamproitic ultrapotassic rocks are relatively uncommon in circum-Mediterranean provinces such as Italy (49.3–58.1 wt.%; Venturelli et al., 1984b, 1988; Peccerillo et al., 1988; Conticelli and Peccerillo, 1992; Conticelli et al., 1992, 2002; Conticelli, 1998) and SE Spain (46.1–60.5 wt.%., Venturelli et al., 1984a, 1991; Turner et al., 1999), exceptions being Jumilla (SE Spain) (SiO_2 = 46.87–

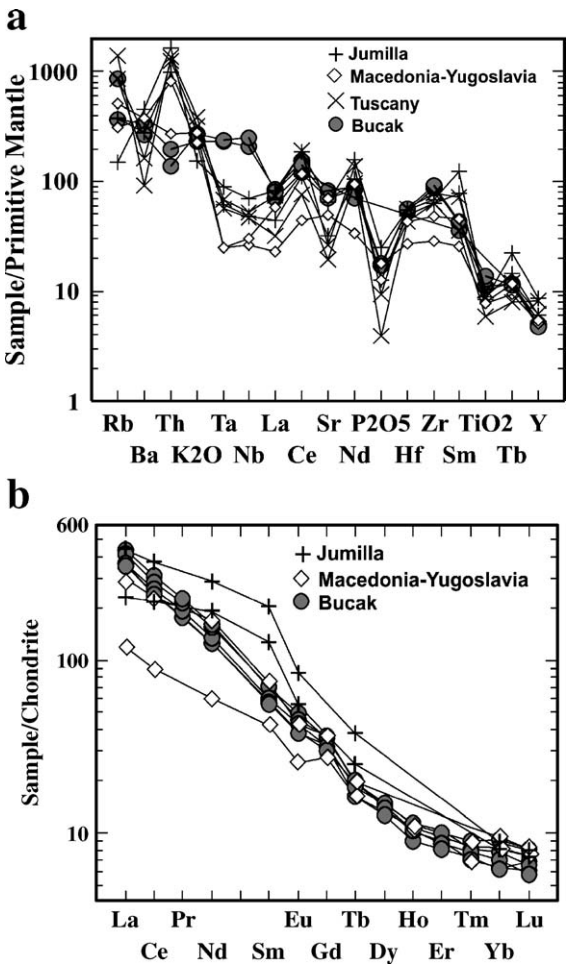

Fig. 6. (a) Spider diagram of the Bucak rocks normalized to primitive mantle, (b) REE condritic patterns of the Bucak rocks. The Jumilla (Venturelli et al., 1991), Tuscany (Conticelli et al., 1992) and Macedonia–Yugoslavia (Altherr et al., 2004) lamproite compositions are reported for comparison. Normalized values after Sun and McDonough (1989).

52.70 wt.%,; Venturelli et al., 1991) and Macedonia–Yugoslavia (East European) (SiO_2=46.8–51.1 wt.%; Cvetkovic' et al., 2004; Altherr et al., 2004). With respect to composition of SiO_2-poor olivine lamproites from West Kimberley, Western Australia (SiO_2=40–44 wt.%; CaO<6 wt.%; Al_2O_3<5 wt.%; MgO>20 wt.%; TiO_2>3 wt.%) (Jaques et al., 1986; Wagner and Velde, 1986), Bucak lamproite major element compositions resemble those of leucite lamproites from the Leucite Hills, Wyoming (SiO_2=49–52 wt.%; Carmichael, 1967) and Gaussberg, Antarctica (SiO_2=43–55 wt.%; Murphy et al., 2002) (Fig. 5b, see also Fig. 14a), and are therefore called 'leucite' lamproite.

Moreover, in contrast to the 'enriched' isotopic compositions of lamproites from Mediterranean occurrences (Spain, Italy, Eastern Europe; Venturelli et al., 1984b; Nelson et al., 1986; Conticelli et al., 1992, 2002; Conticelli, 1998; Turner et al., 1999; Peccerillo, 1999; De Astis et al., 2000; Cvetkovic' et al., 2004; Altherr et al., 2004) ($^{87}Sr/^{86}Sr$, 0.70784–0.7221, $^{143}Nd/^{144}Nd$, 0.5119–0.5124) the Isparta Angle lamproites (e.g. from Bodrum, Denizli, Afyon and Bucak) are characterized by a lower Sr (0.70363–0.7079) and higher Nd (0.5124–0.5128) ratios (Keller, 1983; Gulec, 1991; Robert et al., 1992; Francalanci et al., 2000).

6. Mineral chemistry

Excluding sodalite observed only in one sample, absence of plagioclase and coexisting olivine, phlogopite, diopside, richterite, leucite and sanidine in the matrices of Bucak lamproites are nonetheless typical (Foley et al., 1987; Mitchell and Bergman, 1991) despite the lack of phases such as priderite and wadeite. In contrast to SiO_2-saturated Afyon-Sandikli lamproites (which include phlogopite, K-richterite, olivine, diopside, sanidine, apatite and calcite) ultrapotassic rocks from Denizli and Bodrum reflect significantly higher modal plagioclase. However, MgO-rich SiO_2 undersaturated lamproites from Jumilla in SE Spain (Venturelli et al., 1991) are leucite-free and relatively rich in analcime and carbonates, while those from the Yugoslavia and Macedonia (Eastern Europe) include pseudobrookite-armalcolite, melanite and sphene (Cvetkovic' et al., 2004; Altherr et al., 2004). Mineral phase compositions of the Bucak lamproites are described below.

6.1. Micas

Phlogopites in the Bucak rocks occur as two types (Table 2; Fig. 7), Type I, a high-Mg, Ti poor variety (with Mg#, 85.9–91.6; Al_2O_3, 12.19–14.14 wt.%; Cr_2O_3, up to 1.82 wt.%; FeO, 3.7–6.22 wt.%; TiO_2, 2.15–2.98 wt.%) and Type II, a low-Mg, Ti rich variety occurring as resorbed laths in the groundmass (with Mg#, 70.87–85.6; Al_2O_3, 9.03–13.04 wt.%; Cr_2O_3, up to 0.11 wt.%; FeO, 5.63–11.37 wt.%; TiO_2, 6.25–10.45 wt.%). Type I phologopite is often mantled by Type II, which is Ti rich (6.78–7.11 wt.%), Mg# (85.6–86.6) and Al_2O_3 (11.93–12.1 wt.%) poor (with composition similar to Type II phl) around the Ti poor (2.43–2.51 wt.%), Mg# (89.56–91.6) and Al_2O_3 (13.34–13.4 wt.%) rich core.

Type I mica show notably higher F (1.52–3.25 wt.%) and SiO_2 (39.61–40.84 wt.%) contents, and lower Ba

Table 2
Representative chemical compositions (wt.%) of phlogopites from Bucak lamproites

	Type I phlogopite		Mantled Type I phlogopite		Type II phlogopite	
	Core (N=9)	Rim (N=10)	Core (N=2)	Rim (N=2)	Core (N=18)	Rim (N=11)
SiO_2	40.11	40.71	40.45	39.11	39.44	39.75
TiO_2	2.15	2.47	2.43	6.78	6.25	6.36
Al_2O_3	13.22	12.68	13.34	12.10	10.56	10.48
Cr_2O_3	1.17	0.93	1.19	0.01	<0.01	<0.01
FeO	6.22	4.72	3.87	6.11	5.97	5.63
MnO	0.07	0.04	0.04	0.07	0.08	0.04
MgO	21.26	22.25	23.72	20.45	21.18	21.04
CaO	0.04	0.03	0.01	0.05	0.12	0.07
BaO	0.32	0.23	0.26	2.20	2.11	1.78
Na_2O	1.43	0.41	0.55	0.61	0.49	0.64
K_2O	8.53	9.86	9.74	8.72	9.10	9.02
F	3.25	2.14	2.15	1.92	2.44	1.36
Total	97.44	96.27	97.46	95.93	95.63	94.39
Structural formulas based on 24 oxygens						
Si	5.850	5.798	5.748	5.650	5.754	5.800
Ti	0.266	0.234	0.260	0.736	0.686	0.698
Al	2.146	2.250	2.232	2.058	1.814	1.800
Fe_2	0.568	0.752	0.460	0.738	0.728	0.686
Cr	0.106	0.134	0.134	0.002	–	–
Mn	0.004	0.008	0.004	0.008	0.010	0.004
Mg	4.872	4.580	5.026	4.404	4.608	4.576
Ca	0.004	0.006	0.002	0.008	0.018	0.010
Ba	0.012	0.018	0.014	0.124	0.120	0.102
Na	0.126	0.400	0.152	0.170	0.138	0.182
K	1.766	1.572	1.766	1.608	1.694	1.678
Cations	15.72	15.75	15.80	15.51	15.57	15.54
Mg#	89.56	85.90	91.62	85.65	86.36	86.96
K/Al	0.823	0.699	0.791	0.781	0.934	0.932

FeO=as total Fe, Mg#=(Mg/(Mg+Fe))*100; <: below detection limit; N: number of analyzes; –: not calculated.

(up to 0.4 wt.%) contents relative to Type II micas (F, 0.51–2.67 wt.%; Si, 38.46–39.75 wt.%; Ba, 1.42–3.22 wt.%). Although Types I and II phl display little or no zonation between core and rim compositions, the composition of core of mantled crystals has higher Mg#, Si, Al, F and Cr_2O_3 (0.27–1.19 wt.%) contents and lower Ti and Ba abundances than rims, which are close to Type II phl.

Two types (Type I and Type II) of phlogopite bearing lamproites were also defined from Leucite Hills (Carmichael, 1967), Jumilla (SE Spain; Venturelli et al., 1991), South Tuscany (Italy, Conticelli et al., 1992), and Macedonia and Yugoslavia (East European; Altherr et al., 2004), which show similarity with two types of Bucak micas. Bucak micas display consistency with the micas from typical lamproites and peridotitic xenoliths (Figs. 7 and 8). In contrast, they differ significantly from the micas of Roman province lavas and crustal xenoliths, which are characterized by the higher Al_2O_3 contents (Figs. 7 and 8).

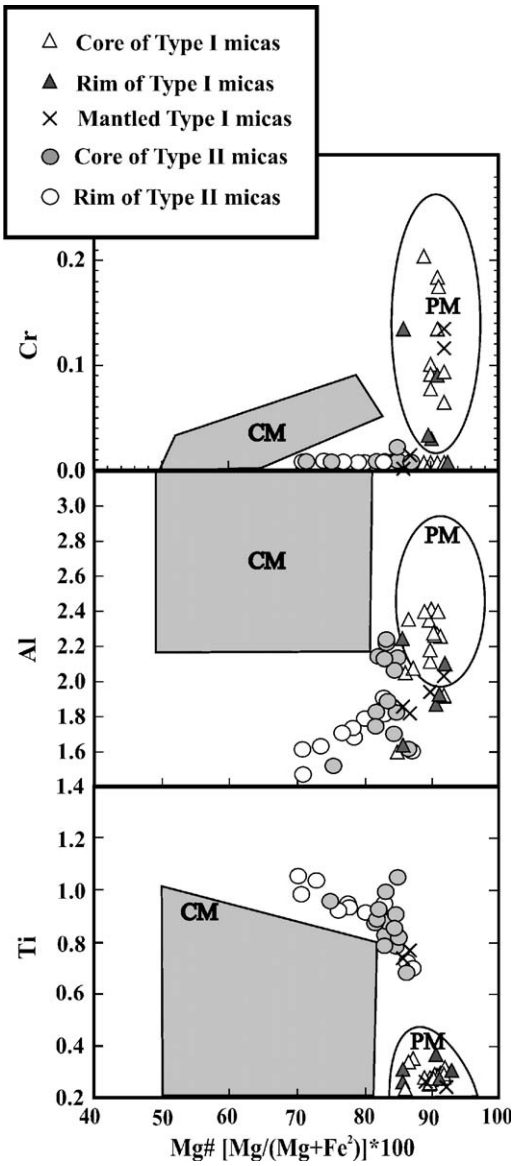

Fig. 7. Ti, Al, Fe and Cr (a.p.f.u.) versus Mg# ($Mg/(Mg+Fe^{2+})$) diagrams of micas from Bucak lamproites, and comparison to micas from peridotite massifs–peridotite xenoliths (PM) and crustal xenoliths (CM). Note that Type I micas fall well within the peridotitic field and Type II phlogopites are not consistent with the composition of crustal micas. Data source for PM and CM; micas in selected granulite xenoliths (Kempton et al., 1995; Conticelli, 1998; Upton et al., 2001; Rickers et al., 2001; Embey-Isztin et al., 2003); in selected veined spinel harzburgite, spinel dunite and garnet peridotite xenoliths (Wulff-Pedersen et al., 1996, 1999; Zhang et al., 2000; Van Achterbergh et al., 2001; Gregoire et al., 2002), and in peridotite massif (Zanetti et al., 1999; Rizzo et al., 2001).

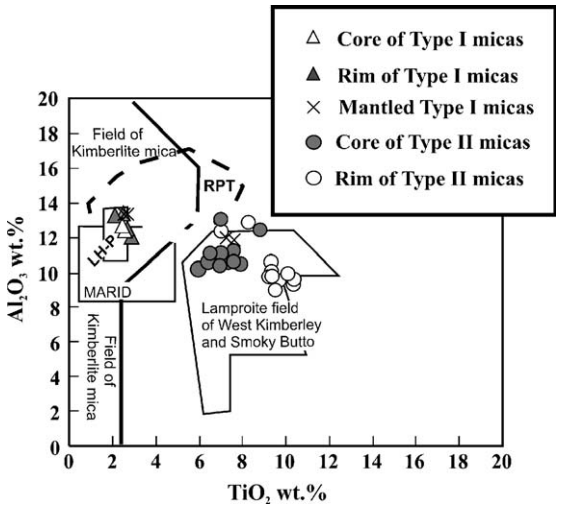

Fig. 8. Variation of TiO_2 (wt.%) and Al_2O_3 (wt.%) in phlogopite from the Bucak lamproites. The fields of phlogopites from kimberlites, selected lamproites and MARID xenoliths are modified from Mitchell and Bergman (1991), and references therein. LH-P: phenocrystal plogopites from Leucite Hills. RPT: phlogopites from Roman Province Types.

6.2. Leucite

Leucite appears as two compositional types in the Bucak lavas: (1) Fe_2O_3-poor (<2 wt.%) and Al_2O_3-rich (21.7–22.78 wt.%) and (2) Fe_2O_3-rich (>2 wt.%) and Al_2O_3-poor (21.26–21.55 wt.%) type (Table 3). In general, high Fe_2O_3 (>1 wt.%) and low Na_2O (0.04–0.09 wt.%), and low CaO (<0.02 wt.%) contents are typical of lamproitic leucites (Mitchell, 1985; Jaques et al., 1986). The high SiO_2 (54.57–56.77 wt.%) and K_2O/Al_2O_3 (0.9–0.97) ratios in the Bucak leucites also indicate their similarity to lamproite leucite, with respect to those in Roman Province lavas (Mitchell and Bergman, 1991).

6.3. Clinopyroxene

Clinopyroxene microphenocrysts, including interstitial crystals in micas and groundmass, cover a wide compositional range (Table 4; Fig. 9), and show high Mg# and Cr (Mg#, 82.53–91.57; Cr_2O_3, up to 1.31 wt.%), low Ti, Na, and Zr contents (TiO_2, 0.68–1.42 wt.%; Na_2O, 0.09–1.76 wt.%; ZrO_2, <0.27 wt.%) diopside cores, Mg#–Cr poor (Mg# 58.57–87.64; Cr_2O_3, <0.35 wt.%), Ti–Na–Zr rich (TiO_2, 0.84–2.93 wt.%; Na_2O, 0.65–6.76 wt.%; ZrO_2, up to 2.62 wt.%) (diopside) augite rims (Table 4; Fig. 9). Core to rim CaO contents (ca. 21.1–23.38 wt.% to ca.14.39–23.1 wt.%) decrease with increasing Fe^{+3} (ca. up to 4.71 wt.% to ca. up to 14.33 wt.%). Al_2O_3 contents in diopsides are low and range from 0.25–1.98 wt.% in cores to 0.35–3.01 wt.% in rims.

The low Al_2O_3 contents of diopsides is characteristic of lamproitic Cpx phase (Cellai et al., 1994; Bindi et al., 1999), and the tetrahedral site of clinopyroxenes in Bucak rocks is usually not filled with Si+Al cation sums which is typically found from that of lamproitic and kamafugitic rocks (Mitchell, 1981; Venturelli et al., 1988; Cellai et al., 1994; Conticelli, 1998; Bindi et al., 1999). Based on the Ti_{total} versus Al_{total} (a.p.f.u) of pyroxene variation diagram from lamproites and Roman Province lavas (modified from Mitchell and Bergman, 1991; Conticelli, 1998; Perini et al., 2000; Perini and Conticelli, 2002), the trend is from core of Bucak clinopyroxene through their rim and fits well with the lamproite field (Fig. 10). Aegirine augites (Mg# 46.73–56.63) have been described as late-stage interstitial plates in Type II phl and in groundmass from Bucak lamproites (Table 4). TiO_2, ZrO_2 and Na_2O contents of these clinopyroxenes exhibit significant variety (TiO_2, 3.94–4.35 wt.%; ZrO_2, 3.91–6.82 wt.%; Na_2O, 8.63–9.07 wt.%). Na-rich aegirine augite was only found in Leucite Hills lamproites (Mitchell and Bergman, 1991) and in

Table 3
Representative chemical compositions (wt.%) of leucites in Bucak rocks

	Low Fe, high Al-bearing leucite		High Fe, low Al-bearing leucite	
SiO_2	55.44	55.77	55.35	54.57
Al_2O_3	21.7	22.78	21.57	21.26
Fe_2O_3	1.57	1.48	2.19	2.27
Na_2O	0.06	0.18	0.06	0.09
K_2O	20.06	20.52	20.4	20.58
CaO	n.a.	n.a.	0.02	<0.01
BaO	0.2	0.13	0.02	<0.01
SrO	n.a.	n.a.	<0.01	0.01
Total	99.03	100.90	99.60	98.78
Structural formulas based on 6 oxygens				
Si	2.035	2.011	2.02	2.015
Al	0.938	0.967	0.927	0.924
Fe	0.048	0.045	0.06	0.063
Na	0.004	0.013	0.004	0.006
K	0.939	0.944	0.95	0.969
Ca	–	–	0.001	–
Ba	0.003	0.013	–	–
Sr	–	–	–	–
Cations	3.967	3.993	3.962	3.977

Fe_2O_3 as total Fe; <: below detection limit; na: not analyzed; –: not calculated.

Table 4
Representative chemical compositions (wt.%) of clinopyroxenes from Bucak rocks

	Core	Rim	Core	Rim	Core	Rim	Core	Rim	Core	Rim	Core	Rim	Interstitials		Inclusions in mica	
SiO_2	52.78	52.94	53.73	53.29	53.06	53.57	53.96	53.68	52.33	53.55	53.10	50.60	51.20	50.71	53.84	53.38
TiO_2	1.05	2.64	1.42	2.83	1.27	2.93	0.82	2.08	1.35	1.79	0.91	1.77	3.94	4.35	1.22	1.25
Al_2O_3	0.81	0.54	0.49	0.62	0.83	0.77	0.25	0.69	1.48	0.35	1.68	3.01	0.71	0.74	0.52	0.72
FeO	1.64	4.16	1.78	0.00	0.56	2.00	1.87	3.08	4.08	3.11	2.13	1.29	0.00	2.29	1.83	1.77
Fe_2O_3	3.37	9.59	4.71	14.33	4.66	11.28	1.81	10.11	0.00	9.10	2.38	6.07	12.48	13.54	3.42	3.55
Cr_2O_3	0.45	0.28	0.16	<0.01	0.21	<0.01	0.13	0.01	<0.01	<0.01	<0.01	<0.01	<0.01	<0.01	<0.01	<0.01
MnO	0.12	<0.01	0.15	0.19	0.14	0.15	<0.01	0.14	<0.01	<0.01	0.24	<0.01	<0.01	<0.01	0.13	0.06
MgO	17.28	10.59	15.93	10.22	17.05	9.78	17.76	11.46	16.59	11.52	17.20	16.00	8.23	7.11	16.65	16.77
CaO	22.01	12.87	21.10	13.18	22.56	12.30	22.96	14.39	23.01	15.26	22.60	21.70	7.86	7.47	22.32	22.21
Na_2O	0.71	5.64	1.76	6.72	0.99	6.76	0.50	5.17	0.09	4.84	0.51	0.98	9.07	8.63	1.13	1.03
ZrO_2	0.25	0.84	<0.01	1.11	<0.01	2.62	<0.01	0.66	0.27	0.45	n.a.	n.a.	6.82	3.91	<0.01	0.06
Total	100.50	100.10	101.20	102.50	101.30	102.20	100.10	101.50	99.20	99.97	101.00	101.00	100.30	98.75	101.10	100.80
Structural formula based on 6 oxygens																
Tsi	1.926	1.979	1.946	1.947	1.916	1.987	1.963	1.972	1.937	1.990	1.930	1.840	1.995	1.983	1.949	1.938
Tal	0.035	0.021	0.021	0.027	0.035	0.013	0.011	0.028	0.063	0.010	0.070	0.130	0.005	0.017	0.022	0.031
Tfe3	0.039	0.000	0.033	0.026	0.048	0.000	0.026	0.000	0.000	0.000	0.000	0.030	0.000	0.000	0.029	0.031
M1Al	0.000	0.003	0.000	0.000	0.000	0.021	0.000	0.002	0.002	0.005	0.000	0.000	0.028	0.017	0.000	0.000
M1Ti	0.029	0.074	0.039	0.078	0.035	0.082	0.022	0.057	0.038	0.050	0.030	0.050	0.115	0.128	0.033	0.034
M1Fe3	0.053	0.270	0.095	0.368	0.078	0.315	0.023	0.279	0.000	0.254	0.060	0.130	0.366	0.398	0.064	0.066
M1Fe2	0.000	0.055	0.001	0.000	0.000	0.042	0.000	0.034	0.045	0.053	0.000	0.000	0.000	0.042	0.004	0.000
M1Cr	0.013	0.008	0.005	0.000	0.006	–	0.004	–	–	–	–	–	–	–	–	–
M1Mg	0.905	0.590	0.860	0.555	0.881	0.541	0.950	0.628	0.915	0.638	0.910	0.820	0.478	0.415	0.898	0.900
M2Mg	0.035	0.000	0.000	0.002	0.037	0.000	0.013	0.000	0.000	0.000	0.020	0.050	0.000	0.000	0.000	0.008
M2Fe2	0.050	0.076	0.053	0.000	0.017	0.020	0.057	0.061	0.081	0.044	0.070	0.040	0.000	0.033	0.051	0.054
M2Mn	0.004	–	0.005	0.006	0.004	0.005	–	0.004	–	–	0.010	–	–	–	0.004	0.002
M2Ca	0.861	0.516	0.819	0.516	0.873	0.489	0.895	0.566	0.913	0.607	0.880	0.850	0.328	0.313	0.870	0.860
M2Na	0.050	0.409	0.124	0.476	0.069	0.486	0.035	0.368	0.006	0.349	0.040	0.070	0.685	0.654	0.080	0.070
Cat.	4.00	4.00	4.00	4.00	4.00	4.00	4.00	4.00	4.00	4.00	4.00	4.00	4.00	4.00	4.00	4.00
Mg#	86.88	59.54	82.53	58.57	86.52	58.93	90.08	62.67	87.90	64.51	87.72	80.92	56.64	46.73	85.85	85.74

Fe^{+2}, Fe^{+3} separation after Droop (1987). Mg#=(Mg/(Mg+Fe))∗100; <: below detection limit; n.a.: not analyzed; –: not calculated.

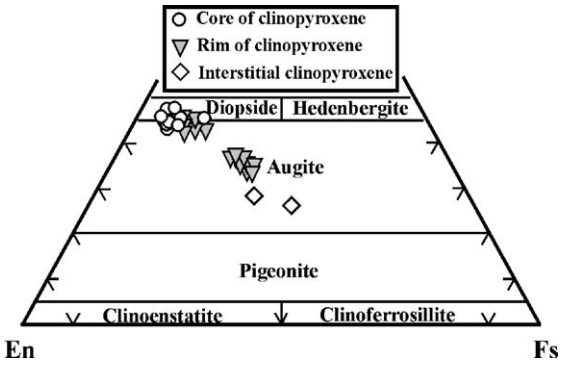

Fig. 9. Diagram of pyroxenes from Bucak lamproites.

Jumilla (SE Spain) silica-undersaturated lamproites (Venturelli et al., 1991).

6.4. Olivine

Olivine in Bucak rocks occur as two types: phenocryst and groundmass microphenocryst, and display consistent zoning (Table 5). Two types of olivine have also been found in Italian (Conticelli, 1998; Conticelli et al., 1992) and French lamproites (Wagner and Velde, 1986). The core of olivine phenocrysts ranges from Fo_{92} to Fo_{90} with rims ranging from Fo_{90} to Fo_{89} (Table 4). Relative to rim (CaO, 0.16–0.22 wt.%; MnO, 0.28–0.47 wt.%), the core has higher MgO, and lower CaO (0.11–0.18 wt. %) and MnO (0.11–0.28 wt.%) contents (Fig. 11). The Fo contents of groundmass microphenocrysts range between 90 and 91, with higher CaO (0.12–0.16 wt. %) and MnO (0.2–0.53 wt.%) contents than phenocryst cores.

6.5. Cr-spinel

Cr-spinels of Bucak lavas are primary spinels falling into the compositional group-2 of the classification of Mitchell (1985) (Table 6). Presence of Cr-spinel inclusions (Cr# Cr/Cr+Al, >90) in olivine is a typical feature of lamproites (Mitchell and Bergman, 1991).

6.6. Amphibole

According to Hawthorne (1983) classification, poiklitic groundmass amphiboles are richterite (Table 7). Although the high Ti and low Na/K contents of lamproite amphiboles appear to be characteristic (Mitchell and Bergman, 1991) (Fig. 12), amphiboles from Bucak and Jumilla lamproites are characterized by relatively high Ti contents and higher Na/K ratios (Table 7).

6.7. Sanidine

Sanidine in Bucak lamproites is a late stage product confined to the groundmass and varies in composition between $Or_{69.1}$ and $Or_{81.5}$ (Table 8). This phase is relatively rich in BaO (0.95–2.76 wt.%), Na_2O (2.01–3.16 wt.%) and Fe_2O_3 (1.66–2.40 wt.%) and poor in SrO (up to 0.58 wt.%), and in common with those from Jumilla lamproites, are characterized by relatively low CaO contents (0–0.045 wt.% for Bucak; <0.06 wt.% for Jumilla), compared to most other circum-Mediterranean lamproites (>0.5) (Conticelli, 1998).

6.8. Fe–Ti oxides

Two types of magnetite, Cr-rich and Cr-poor, may be recognized in the Bucak lavas (Table 9), occurring as inclusions in phlogopite and in the groundmass and showing resorption textures. However, there is no apparent correlation of these with Fe, Al, and Ti variation, or with ulvospinel content (Fig. 13), raising the possibility that they result from breakdown of phlogopites (see Petrography). Ilmenite is also present as late stage groundmass phase (Table 9).

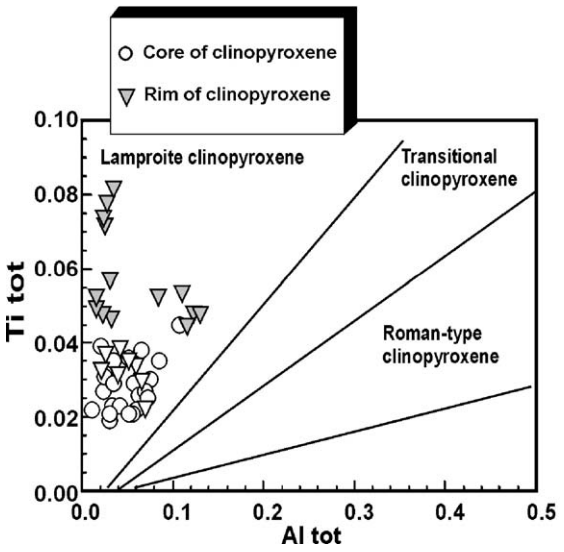

Fig. 10. Al_{total} versus Ti_{total} expressed as atoms per formula unit (a.p.f.u.) for clinopyroxenes from Bucak lavas. Lamproite and Roman Province fields are adapted from Mitchell and Bergman (1991), Conticelli (1998), Perini et al. (2000) and Perini and Conticelli (2000).

Table 5
Representative chemical compositions (wt.%) of olivines in Bucak rocks

	Phenocrystal						Groundmass microphenocrystal		
	Core	Rim	Interval	Rim	Core	Interval	Core	Core	Core
SiO_2	41.22	41.29	41.15	41.29	41.23	41.30	41.23	40.63	40.96
TiO_2	0.01	0.04	<0.01	0.02	0.02	0.01	<0.01	<0.01	0.04
Al_2O_3	0.02	0.03	0.02	0.02	0.02	0.02	0.03	0.04	0.02
Cr_2O_3	0.09	0.08	0.10	0.07	0.12	0.06	0.10	0.07	0.03
FeO	8.46	8.93	9.39	8.92	7.69	8.26	8.82	8.89	8.66
MnO	0.29	0.43	0.20	0.28	0.16	0.23	0.38	0.45	0.29
MgO	48.30	47.94	48.89	49.20	49.88	49.49	48.89	48.55	48.60
CaO	0.17	0.19	0.13	0.16	0.12	0.11	0.15	0.12	0.14
Na_2O	0.05	0.04	<0.01	<0.01	0.02	0.01	0.05	0.04	0.01
K_2O	0.01	0.01	0.01	0.01	<0.01	<0.01	0.01	<0.01	<0.01
Total	98.71	99.09	99.99	99.97	99.46	99.90	99.84	98.95	98.98
Structural formula based on 4 oxygens									
Si	1.016	1.017	1.006	1.007	1.006	1.007	1.008	1.004	1.009
Al	0.001	0.001	0.001	0.001	0.001	0.001	0.001	0.001	0.001
Cr	–	–	–	–	–	–	–	–	–
Ti	–	0.001	–	–	–	–	–	–	0.001
Fe_2	0.174	0.184	0.192	0.182	0.157	0.168	0.180	0.184	0.178
Mn	0.006	0.009	0.004	0.006	0.003	0.005	0.008	0.009	0.006
Mg	1.775	1.760	1.782	1.789	1.815	1.799	1.782	1.788	1.785
Ca	0.004	0.005	0.003	0.004	0.003	0.003	0.004	0.003	0.004
Na	0.002	0.002	–	–	0.001	–	0.002	0.002	–
K	–	–	–	–	–	–	–	–	–
Cat.	2.98	2.98	2.99	2.99	2.99	2.99	2.99	2.99	2.99
Mg#	91.07	90.53	90.27	90.77	92.04	91.46	90.83	90.67	90.93

FeO as total Fe, Mg#=(Mg/(Mg+Fe))∗100; <: below detection limit; –: not calculated.

6.9. Apatite

Abundant apatite occurs as prismatic, needle-like microphenocrysts in the groundmass as well as inclusions in phlogopites. Analyzed apatites show CaO contents of 53.23 wt.%, P_2O_5, 43.8 wt.% and SrO, 2.97 wt.%.

6.10. Other accessory phases

Sodalite, unusual and nonobserved mineral in lamproites, was only found in the altered groundmass of one sample, showing contents of Na_2O 8.63–9.07 wt. %, Cl 6.46 wt.%, Al_2O_3 30.81 wt.%, SiO_2 41.35 wt.%, and K_2O 1.78 wt.%. Other accessory phases include

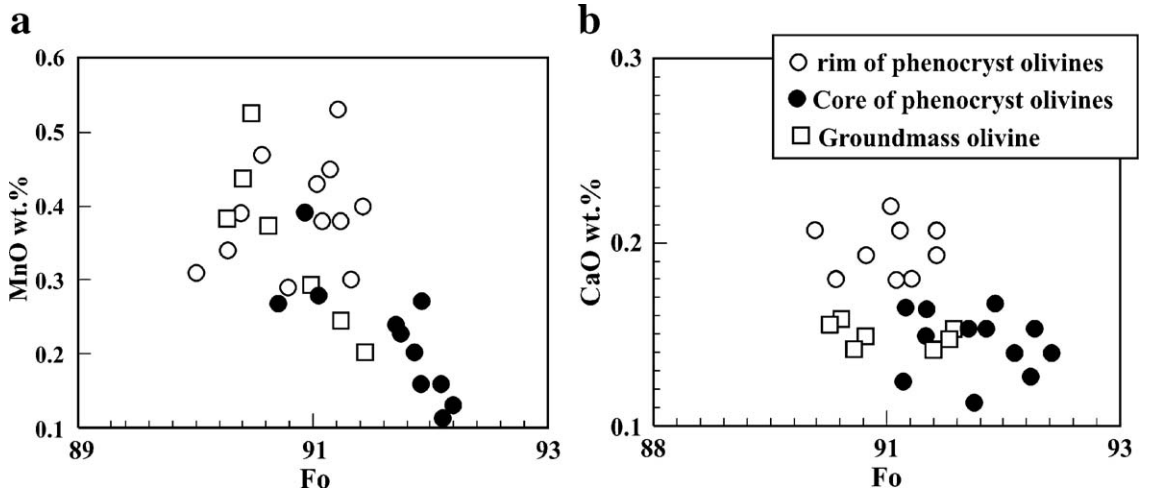

Fig. 11. Diagrams of Fo versus (a) CaO (wt. %), and (b) Mn (wt. %) variation in olivines from Bucak lavas.

Table 6
Representative chemical compositions (wt.%) of Cr-spinels in olivine from Bucak rocks

SiO_2	0.21	0.08	0.11	0.08	0.20	0.07	0.03	0.07
TiO_2	1.28	1.22	1.26	1.20	1.26	1.40	1.31	1.09
Al_2O_3	3.51	3.38	3.41	3.23	3.21	3.88	3.72	2.92
FeO	18.62	17.46	18.46	17.44	19.77	19.44	18.15	18.03
Fe_2O_3	8.15	9.91	9.14	9.67	7.95	7.85	9.59	10.05
Cr_2O_3	55.95	54.79	55.45	54.24	58.13	57.66	55.16	53.77
MnO	0.28	0.28	0.31	0.26	0.26	0.23	0.32	0.28
MgO	9.13	9.71	9.22	9.48	9.48	8.78	9.37	9.85
CaO	0.06	0.02	0.04	0.02	0.03	0.04	0.02	0.02
Na_2O	<0.01	0.01	0.03	0.01	<0.01	0.01	0.04	0.01
Total	97.19	96.86	97.43	95.63	100.30	99.36	97.71	96.09
Structural formulas based on 4 oxygens								
Si	0.007	0.003	0.004	0.003	0.007	0.002	0.001	0.003
Al	0.146	0.140	0.141	0.136	0.129	0.158	0.153	0.123
Ti	0.034	0.032	0.033	0.032	0.032	0.036	0.034	0.029
Fe_2	0.548	0.515	0.543	0.521	0.566	0.561	0.531	0.538
Fe_3	0.216	0.263	0.242	0.260	0.205	0.204	0.252	0.270
Cr	1.556	1.525	1.540	1.531	1.572	1.571	1.524	1.515
Mn	0.008	0.008	0.009	0.008	0.008	0.007	0.009	0.008
Mg	0.479	0.510	0.483	0.505	0.484	0.452	0.489	0.524
Ca	0.002	0.001	0.002	0.001	0.001	0.001	0.001	0.001
Na	–	0.001	0.002	0.001	–	0.001	0.003	0.001
Cations	2.997	2.998	2.999	2.998	3.004	2.993	2.997	3.012
Cr#	0.914	0.916	0.916	0.918	0.924	0.909	0.909	0.925

Cr#=Cr/(Cr+Al); <: below detection limit; –: not calculated.

small quantities of (unidentified) calcium–titanium niobate.

7. Discussion

7.1. Petrogenetic implications

A detailed interpretation of the lamproitic whole-rock compositions is presented separately (Coban and Flower, in press). However, before discussing petrogenetic implications of the mineral data, whole-rock variation is briefly reviewed in terms of relevant experimental studies. Such studies have concluded that SiO_2-undersaturated lamproites represent partial melts of refractory, phlogopite-bearing, peridotite under H_2O-saturated or undersaturated conditions at pressures up to ca. 5 GPa (Luth, 1967; Wendlandt and Eggler, 1980; Foley, 1989a,b; Foley et al., 1986a,b). Projections of the Bucak whole-rock compositions on to the Ks–Fo–Qz and Ne–Fo–Qtz planes in the Ks–Fo–Qz–Ne system (cf. Luth, 1967; Wendlandt and Eggler, 1980; Foley, 1989a) (Fig. 14a and b) plot close to the experimental H_2O-saturated phlogopite–harzburgite peritectic (involving incongruent melting of phlogopite) between pressures of ca. 1.7 and 2.0 GPa, equivalent to depths of about 50−60 km (Foley et al., 1986a). In contrast, projections of IAUP whole-rock compositions indicate magma segregation pressures of ca. 1–1.5 GPa (ca. 30–45 km depth).

7.1.1. Thermobarometry: high pressure and low pressure phases

In general, SiO_2-undersaturated melts have been interpreted to reflect combined effects of relatively high total pressure and/or high PCO_2 ($\pm F/H_2O$) rather than PH_2O (e.g. Foley et al., 1986b). The analyzed Bucak lamproitic phase compositions provide thermobarometric constraints on magmatic crystallization conditions. For example, the relatively low Ca and Mn contents of olivine cores relative to their rims (at both high and low temperatures) suggest that crystallization occurred over a range of pressure conditions (Simkin and Smith, 1970; Adams and Bishop, 1986; Kohler and Brey, 1990). Geobarometers based on Cr-spinel composition (e.g. O'Neill, 1981; Web and Wood, 1986) and using the PERIDOT algorithm (Nasir, 1996) indicate that Cr-spinel began crystallizing between 1.7 and 2.0 GPa, and ca. >1 GPa interpreted from coexisting olivine (Kohler and Brey, 1990). Mg# and Cr# values in the Bucak Cr-spinels resemble those of (higher pressure) kimberlite- rather than (lower pressure) alkali basalt-born xenoliths (Basu and McGregor, 1975), confirming

Table 7
Representative chemical compositions (wt.%) of amphiboles from Bucak lamproites

SiO_2	53.01	54.36	53.81	50.98	52.46
TiO_2	3.09	2.63	3.57	5.82	5.01
Al_2O_3	1.82	1.69	2.12	2.26	2.18
Cr_2O_3	0.16	<0.01	<0.01	<0.01	<0.01
FeO	6.15	6.20	6.61	7.79	6.77
MnO	0.06	0.08	0.12	0.05	0.19
MgO	19.33	19.41	18.69	17.17	17.87
CaO	4.86	4.64	4.48	5.03	5.35
Na_2O	7.22	7.27	6.93	6.79	6.62
K_2O	1.79	1.84	1.94	2.38	2.01
F	1.43	1.21	1.95	1.06	0.76
Total[a]	97.49	98.12	98.27	98.27	98.46
Structural formula based on 23 oxygens					
TSi	7.552	7.668	7.593	7.312	7.439
TAl	0.305	0.281	0.352	0.382	0.364
TTi	0.143	0.051	0.055	0.306	0.197
CTi	0.188	0.228	0.324	0.322	0.337
CCr	0.018	–	–	–	–
CFe2	0.733	0.731	0.780	0.934	0.803
CMn	0.007	0.010	0.014	0.006	0.023
CMg	4.106	4.082	3.932	3.671	3.777
BCa	0.742	0.701	0.677	0.773	0.813
BNa	1.258	1.299	1.323	1.227	1.187
ANa	0.737	0.690	0.573	0.661	0.633
AK	0.325	0.331	0.349	0.435	0.364
Cations	16.11	16.07	15.97	16.03	15.94
Mg#	84.85	84.81	83.45	79.72	82.47

FeO=as total Fe. [a]Total does not include F. Mg#=(Mg/(Mg+Fe$_2$))∗100; <: below detection limit; –: not calculated.

their relatively high pressure (>1.0 GPa) origins. Olivine core crystallization temperatures (ca. 920–1050 °C) are higher than those (ca. 850–950 °C)

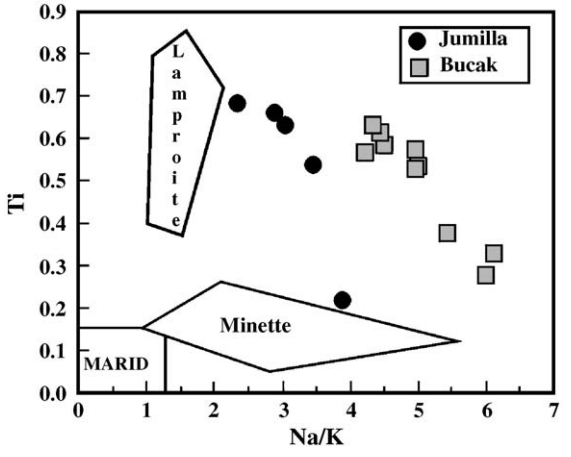

Fig. 12. Ti–Na/K (expressed as a.p.f.u.) variations of composition of amphiboles in Bucak lamproites. MARID, Minette and lamproite fields modified from Mitchell and Bergman (1991). Amphibole compositions from Jumilla (SE Spain, Venturelli et al., 1991) lamproites are reported for comparison.

Table 8
Representative chemical compositions (wt.%) of K-feldspars from Bucak rocks

SiO_2	63.46	63.87	62.62	63.69	63.88
Al_2O_3	18.04	18.41	18.71	18.32	18.04
Fe_2O_3	2.40	1.66	1.79	1.66	2.03
BaO	1.81	1.77	2.76	1.74	0.95
CaO	n.d.	0.05	0.01	0.03	n.d.
Na_2O	2.32	3.16	3.07	3.10	2.01
K_2O	12.42	10.88	10.44	11.09	13.46
SrO	n.a.	0.31	0.58	0.21	n.a.
Total	100.50	100.10	99.98	99.83	100.40
Structural formula based on 8 oxygens					
Si	2.957	2.952	2.923	2.953	2.967
Al	0.990	1.002	1.028	1.000	0.987
Fe	0.094	0.058	0.063	0.058	0.079
Ba	0.033	0.032	0.050	0.032	0.017
Ca	n.d.	0.002	0.000	0.001	n.d.
Na	0.210	0.283	0.278	0.279	0.181
K	0.738	0.642	0.622	0.656	0.797
Sr	n.a.	0.008	0.016	0.006	n.a.
Cations	5.022	4.98	4.98	4.99	5.03
Ab	22.20	30.50	30.90	29.80	18.50
An	0.00	0.20	0.00	0.10	0.00
Or	77.80	69.30	69.10	70.10	81.50

Fe_2O_3=as total Fe; n.a.: not analyzed; n.d.: not determined.

estimated for their rims (e.g. O'Neill and Wall, 1987; Ballhaus et al., 1991).

Experimental studies of phlogopite in the pressure range 1.0–5.0 GPa indicate that Ti, Cr, and BaO contents decrease with increasing pressure (Forbes and Flower, 1974; Arima and Edgar, 1983; Foley, 1989b, 1990, 1993; Righter and Carmichael, 1996; Konzet, 1997). While contents of these elements in the Bucak Type I phlogopites are lower than those in Type II micas, they are significantly higher than in phlogopites reported from garnet–peridotite and olivine lamproite (Carswell, 1975; Dawson and Smith, 1977; Delaney et al., 1980; Foley, 1989a,b). This suggests that the Bucak Type I micas probably began crystallizing at pressures of ca. 1.0–2.0 GPa, equivalent to upper mantle (cf. Foley, 1989a,b, 1993) prior to their resorption and mantling by Type II phlogopite (at ca. 1.0–0.5 GPa).

The presence of apatite as inclusions in the latter indicates their early appearance, more or less contemporaneous with Type I phlogopite, in the crystallization sequence (Haggerty et al., 1994; Green, 1995).

Cr# and Mg# of pyroxenes strongly depend on pressure (Thompson, 1974; Ramsay, 1992; Nimis, 1998). Nimis (1995) geobarometer was estimated on clinopyroxenes in Bucak rocks, and pressures obtained range between 1.05 and 0.1 GPa (from core to rim). According to Foley (1989b), crystallization of clinopyroxene in leucite lamproites is restricted with 0.5 GPa,

Table 9
Representative chemical compositions (wt.%) of Fe–Ti oxides from Bucak rocks

	Magnetites in phlogopites			Magnetites in groundmass										
TiO_2	9.83	10.84	8.68	10.27	8.55	7.76	5.16	4.38	7.41	7.14	10.24	12.45	11.95	12.72
Al_2O_3	0.05	0.07	0.36	0.13	0.36	0.48	0.20	0.28	0.08	0.06	0.06	0.00	0.00	0.00
FeO	34.99	36.80	33.03	34.89	33.23	33.50	28.87	27.64	28.82	29.35	36.32	37.29	39.12	38.19
Fe_2O_3	47.77	45.04	50.73	48.07	49.25	52.90	57.83	58.10	51.98	52.48	47.50	42.07	43.33	41.01
Cr_2O_3	1.65	1.33	1.66	1.12	2.60	2.15	0.11	1.21	0.40	0.41	0.91	0.04	0.12	0.57
MnO	0.79	1.08	0.70	0.92	0.79	0.65	0.68	0.62	1.36	1.36	0.72	1.14	0.98	1.48
MgO	2.17	1.27	2.95	2.75	2.71	2.77	3.23	3.51	3.62	3.13	1.64	0.50	0.36	0.75
Total	97.46	96.58	98.29	98.20	97.59	100.20	96.40	96.01	93.81	94.10	97.63	94.09	96.01	95.19
Structural formula based on 4 oxygens														
Al	0.002	0.003	0.016	0.006	0.016	0.021	0.009	0.013	0.004	0.003	0.003	0.000	0.000	0.000
Ti	0.284	0.318	0.247	0.293	0.245	0.217	0.150	0.128	0.220	0.212	0.296	0.375	0.355	0.379
Fe_2	1.124	1.200	1.045	1.107	1.061	1.043	0.933	0.895	0.952	0.971	1.169	1.250	1.292	1.265
Fe_3	1.379	1.320	1.443	1.371	1.413	1.480	1.680	1.691	1.544	1.561	1.375	1.268	1.287	1.221
Cr	0.050	0.041	0.050	0.034	0.078	0.063	0.003	0.037	0.012	0.013	0.028	0.001	0.004	0.018
Mn	0.026	0.036	0.022	0.030	0.026	0.020	0.022	0.020	0.046	0.046	0.023	0.039	0.033	0.050
Mg	0.124	0.074	0.166	0.156	0.154	0.154	0.186	0.203	0.213	0.185	0.094	0.030	0.021	0.044
Cations	2.999	2.999	2.998	2.999	2.999	2.998	2.996	3.000	2.997	3.000	2.998	3.000	2.999	3.000
Ilmenite														
TiO_2	50.73	50.21	50.46											
FeO	39.65	38.49	39.24											
Fe_2O_3	6.96	8.40	7.52											
MgO	3.35	3.74	3.44											
Total	100.70	100.80	100.70											
Structural formula based on 3 oxygens														
Ti	0.94	0.92	0.93											
Fe_2	0.81	0.79	0.81											
Fe_3	0.13	0.15	0.14											
Mg	0.12	0.14	0.13											
Cations	2.00	2.00	2.00											

implying, by analogy, that the Bucak clinopyroxenes crystallized at relatively low pressures, consistent with petrographic observation of their growth at the expense of phlogopite. Relatively high TiO_2 contents of aegirine also suggest crystallization temperatures of <600 °C (Ferguson, 1977).

Erlank et al. (1987) emphasized that agpaitic index (K+Na/Al) of K-richterite is ≫1 (up to 8) indicating the dominant role in the mantle source. However, Bucak amphiboles contain lower K range between 0.32 and 0.43 a.p.f.u. (Table 7). The major compositional trend in the Ti-bearing amphiboles is an increase in K pfu from 0.67 at 1.0 GPa/900 °C to 1.03 at 8.0 GPa/1100 °C (Konzet, 1997). Thus, Bucak amphiboles were probably crystallized under the low P/T conditions (less than 1.0 GPa/900 °C). Konzet (1997) indicate that Ti in amphibole decreases continuously with increasing pressures. TiO_2 of the low K-richterites from Bucak lava range between 2.63 and 5.73 wt.%, that indicate also low pressure crystallization conditions.

Experimental studies in Ks–Fo–Si suggest that leucite appears as a reaction product of phlogopite at pressures of ca. 0.3 GPa or less (Luth, 1967) while experimental data for the Or–Ab–An system indicate sanidine may also be a late-stage breakdown product of phlogopite at relatively low temperatures (ca. 600–700 °C). Oxides are possibly derived from breakdown of phlogopites as late-stage phases.

In general, core to rim compositional variation trends in the analyzed Bucak mineral phases indicate a polybaric crystallization history, commencing with Cr-spinel, olivine, Type I phlogopite, and apatites at pressures of ca. 1.0–2.0 GPa, followed by the appearance of Type II phlogopite, clinopyroxene, K-poor richterite, leucites, sanidines, and other minor phases at pressures of ca. 0.1–1.0 GPa (Table 10).

7.1.2. Oxygen fugacity

Estimates of ambient magmatic oxygen fugacity (fO_2) can be derived from phlogopite and Cr-spinel

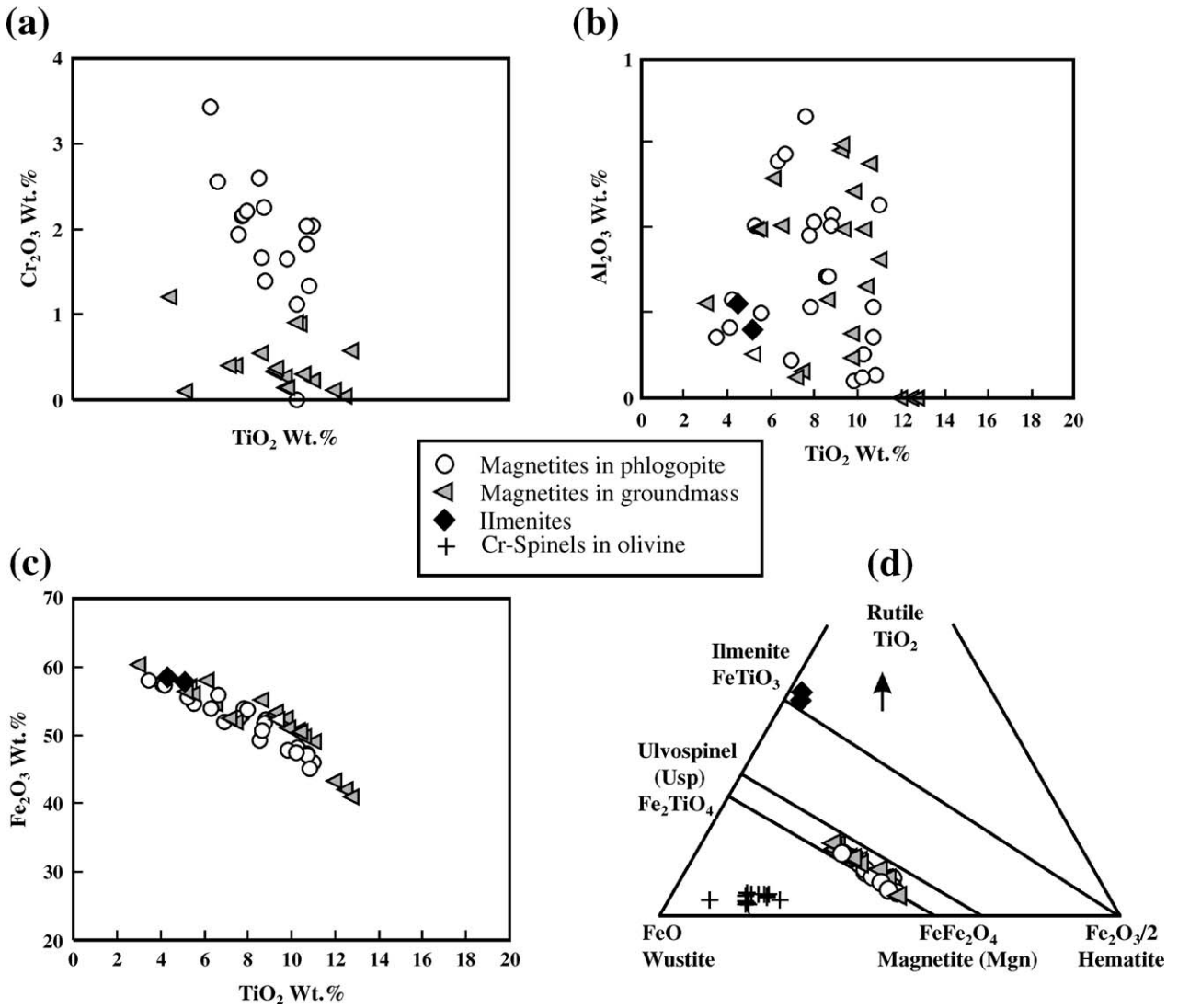

Fig. 13. Plots of several major elements (a, b, c and d) showing magnetite compositions in Bucak rocks. The field of Usp-Mt (d) is after Spencer and Lindsley (1981).

compositions (Mitchell and Bergman, 1991; Foley et al., 1986b; Foley, 1989b, 1992b). Average K_2O/Al_2O_3 ratios ranging from 0.79 to 0.88 in Types I and II phlogopites and $Fe^{+3}/\sum Fe$ ratios in Cr-spinel inclusions ranging from 0.26 to 0.34, close to mode at 0.30±0.05 (Ballhaus et al., 1991), indicate fO_2 conditions between those of the QFM and Ni–NiO buffers, while fO_2 estimates based on coexisting olivine–spinel compositions (Ballhaus et al., 1991; Nell and Wood, 1991) are equivalent to +2 log fO_2 units. These data are in agreement with those found for ultrapotassic magmas from phlogopite-bearing sources. Additionally, relative enrichment in Na and Fe^{+3} and depletions in Ca and Fe^{+2} in aegirine-rich pyroxenes are also consistent with fO_2 conditions exceeding those of the QFM buffer at late stage (Nash and Wilkinson, 1970; Stephenson and Upton, 1982), while the observed enrichment in Zr may be attributed to its high solubility, along with F, in peralkaline melts (Watson, 1979; Collins et al., 1982; Kogarko and Lazutkina, 1988). Rapid equilibrium crystallization may have further facilitated Zr partitioning into interstitial aegirine-rich pyroxenes (Duggan, 1988), reflecting the combined roles of oxygen fugacity and peralkalinity.

7.1.3. Magmatic phase equilibria

Establishing whether olivine phenocrysts had equilibrated with primitive lamproitic melt, their analyzed compositions can be compared with those inferred from

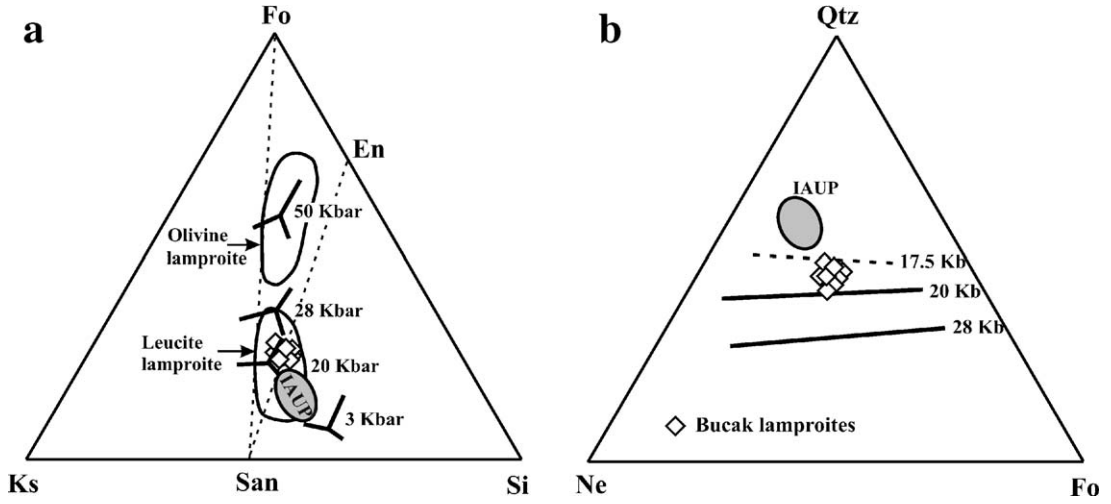

Fig. 14. Projection for compositions of Bucak and Isparta Angle ultrapotassic rocks (IAUP) (a) in the $KAlSiO_4$–Mg_2SiO_4–SiO_2 system and (b) in the $NaAlSiO_4$–Mg_2SiO_4–SiO_2 system. Data sources: for Ks–Fo–Si projection after Foley et al. (1986a), Foley (1989a,b), Gupta and Green (1988) and Luth (1967). For Ne–Fo–Qtz projection after Foley et al. (1986a,b) (references therein); for other Isparta Angle ultrapotassic rocks having lamproitic affinity (assuming MgO > 3 wt %, Al_2O_3 < 13 wt % and K_2O/Na_2O > 1.5), after Besang et al. (1977), Keller (1983), Ercan et al. (1983, 1985, 1996), Gulec (1991), Robert et al. (1992), Aydar et al. (1996) and Akal and Helvaci (2002).

experimental partitioning data for Mg and Fe^{+2}, i.e. $K_D = 100 * ((Fe^{+2}/Mg)_{Ol} * (Mg/Fe^{+2})_{Liq}) = 0.29 \pm 0.03$ (Roder and Emslie, 1970; Roder, 1974; Ulmer, 1989; Grove and Juster, 1989). K_D values interpolated for the Bucak olivines range between 0.29–0.33 (for Cr-spinel bearing olivine cores) and 0.34–0.42 (for phenocryst rim and groundmass olivines), suggesting that only Cr-spinel-bearing olivine cores were in equilibrium with the host magma. Fo–Cr# covariance in both chromite and olivine core compositions fall within or close to the olivine–spinel mantle array (OSMA) (Arai, 1994) (Fig. 15). The correspondence of high Cr# and low Al_2O_3 (2.92–3.88 wt.%) in Cr-spinels, and high olivine Fo contents (Fo_{92-91}) thus strongly suggest that the erupted Bucak lamproites represent primary or near-primary partial melts of a relatively refractory peridotite source (cf. Jaques and Green, 1980; Arai, 1999; Kamenetsky et al., 2001; Green et al., 2001), similar to that of Italian lamproites (Conticelli et al., 2004).

Table 10
Summary of the polybaric crystallization conditions of mineral phases in Bucak lamproites

High-pressure (2.0–1.0 GPa)	Low-pressure (1.0–0.1 GPa)
Cr-spinel	Type II phlogopite
Olivine	Clinopyroxene
Type I phlogopite	K-poor richterite
Apatite	Leucite
	Sanidine
	Fe–Ti oxides

The Bucak Type I phlogopites resemble those from peridotite xenoliths rather than aluminous micas in magmas affected by crustal wall rock reaction (see Fig. 7) (e.g. Brigatti and Gregnanin, 1987) while Cr_2O_3 versus TiO_2 covariance in the Type I phlogopites is similar to that of metasomatic phlogopites in xenoliths entrained by kimberlites (e.g. Aoki, 1975; Carswell, 1975; Dawson and Smith, 1977; Smith et al., 1979; Delaney et al., 1980; Harte et al., 1987; Erlank et al., 1987; Gregoire et al., 2002), olivine nephelinites (Wagner et al., 1996), olivine lamproites (Mitchell and Bergman, 1991; Conticelli, 1998), alkali basalts (Ionov and Hofmann, 1995) and massif peridotites (Zanetti et al., 1996; Rizzo et al., 2001) (Fig. 16).

According to experimental evidence (Foley et al., 1986a; Foley, 1989a,b, 1990, 1992a, 1993), with increasing fO_2 and/or increasing pressure, the contents of Al_2O_3 and BaO in micas increase and those of SiO_2, K_2O, and F decrease. The TiO_2 content of phlogopite also increases significantly with fO_2 under more oxidizing conditions (Foley, 1989b, 1993). Micas in Bucak lava show significant differences among Al, Ba, K/Al, F and Si ratios (Table 2; see also Mineral chemistry). While Type I micas have relatively lower Ba, K/Al (0.9–0.7; mean, 0.79) and higher F, Al and Si (≈39.61–40.8 wt.%), Type II phl and rim of mantled Type I micas have higher K/Al (1.06–0.7; mean, 0.88) and lower F, Ba and Si (≈38–39.5 wt.%) ratios (Table 2; Figs. 7 and 17). Since Type I phl from the Bucak lamproite show higher contents of Al, Ti, F and Si and lower Ba contents than those of Type II phl, it was

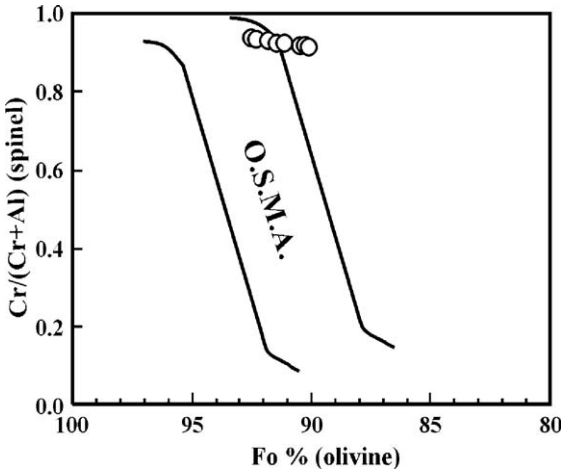

Fig. 15. Variation diagram of Cr/(Cr+Al) in spinel inclusions versus the Fo content of olivines from Bucak lavas. The field of olivine spinel mantle array (O.S.M.A.) is drawn after Arai (1994).

probably equilibrated at higher oxygen fugacities than the latter. Thus, the chemical transition from Type I to Type II phl cannot be explained by the increasing fO_2. As mentioned above (see Thermobarometry: high pressure and low pressure phases), it is suggested that change in the crystallization pressure of micas probably played a more important role than fO_2. The rim of mantled Type I phl, and Type II phl show a sharp decrease in Al, with respect to Type I phl (see Fig. 7). This type of trend, for which Al_2O_3 abundances in mica decrease sharply, was

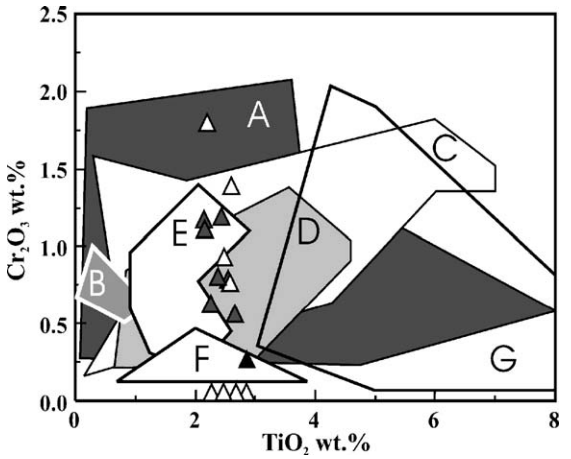

Fig. 16. TiO_2 (wt.%) versus Cr_2O_3 (wt.%) diagram of Type I phlogopites in Bucak lamproites. Fields adapted from Rizzo et al. (2000) (references therein). (A, B) Mica from peridotite xenoliths in kimberlite; (C) mica from Horoman peridotite complex; (D) mica from veined peridotite xenoliths in kimberlite from Bultfontein; (E) mica from Serre ultramafic rocks; (F) mica nodules and MARID xenoliths in kimberlite; (G) mica from ultramafic–mafic xenoliths in basalt from Kerguelen Islands. Symbols as in Fig. 7.

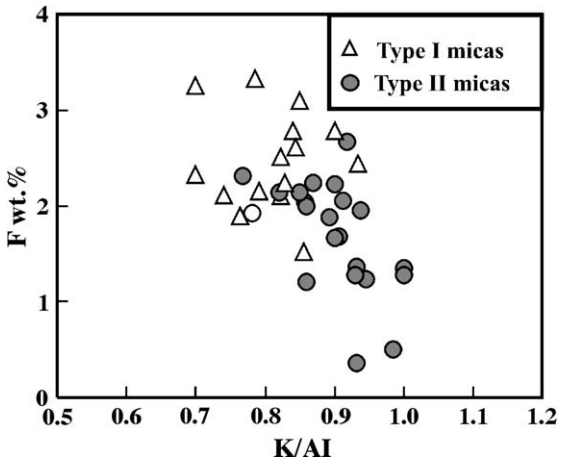

Fig. 17. K/Al versus F (wt.%) variations of composition of Type I and Type II phlogopites in Bucak lamproites.

also found in West Kimberley, Smoky Butto and Spanish lamproites (Mitchell, 1981, 1985; Jaques et al., 1986) and was attributed by Foley (1990) to relatively H_2O-rich conditions.

The Mg# (79.7–84.5) of Bucak amphiboles are close to Mg#'s expected from the amphiboles in equilibrium with mantle peridotite (Aoki, 1975; Sudo and Tatsumi, 1990; Foley, 1991; Zanetti et al., 1996; Niida and Green, 1999; Tieopolo et al., 2000).

The Cr-rich diopsidic clinopyroxenes in Bucak lamproites resemble those in metasomatic PKP (Phlogopite–K-richterite–Peridotite) and MARID (Mica–Amphibole–Rutile–Ilmenite–Diopside) xenoliths (Fig. 18),

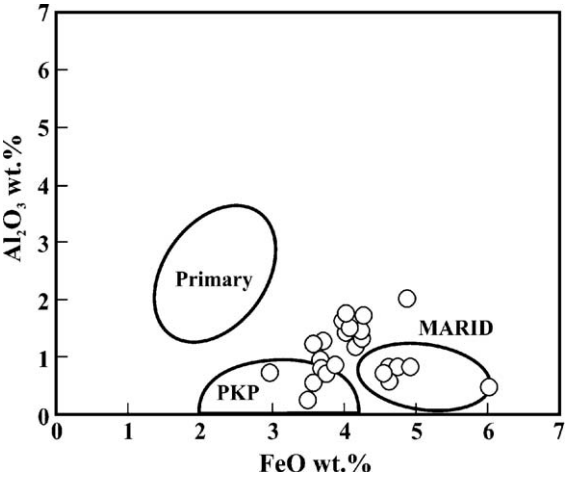

Fig. 18. Al_2O_3 (wt.%) versus FeO (wt.%) plot of the clinopyroxenes (open circle) from Bucak lamproites. Primary, PKP (phlogopite/K-richterite-bearing peridotites) and MARID fields after Wagner et al. (1996) (references therein).

their low Al_2O_3 contents suggesting strongly depleted, metasomatized spinel lherzolite (rather than garnet–lherzolite) sources (Nimis, 1998).

8. Summary and conclusions

Pliocene lamproitic volcanism in Bucak, southwestern Turkey marks a late stage of post-collision igneous activity in the Afyon-Isparta ultrapotassic province, associated with extensional thinning of the lithosphere (Saunders et al., 1998) and the development of shallow asthenosphere (Ilkisik, 1997; Bayrak and Nalbant, 2001, Al-Lazki et al., 2004). The lamproites comprise magmatic assemblages of Cr-spinel, olivine, Type I and Type II phlogopite, diopsidic pyroxene, richterite, leucite, sanidine and Fe–Ti oxides. Whole-rock geochemical features (e.g. Mg# ranging from 73 to 75) suggest the Bucak lamproites represent primary (or near-primary) SiO_2-undersaturated, ultrapotassic magmas, essentially unaffected by crustal wall rock contamination (e.g. low Sr-isotope ratios, 0.70385; steep REE patterns; low Th contents and absence of negative Nb anomaly), formed by partial melting of metasomatized, refractory peridotite.

The presence of phlogopite and amphibole indicate relatively high contents of H_2O and F while analogue experimental studies suggest that these magmas were generated by H_2O-saturated, incongruent melting of phlogopite–harzburgite, at pressures of ca. 1.7 and 2.0 GPa (ca. 50–60 km depth (e.g. Foley et al., 1986a)). In contrast, projections of SiO_2-saturated lamproite compositions from Afyon, to the north, indicate magma segregation pressures of ca. 1–1.5 GPa (ca. 30–45 km depth). While the source composition and pressure of partial melt segregation were clearly dominant factors determining the SiO_2-undersaturated character of Bucak lamproites, petrographic relationships and mineral phase compositional variation strongly suggest the effects of polybaric crystallization, early appearance of Cr-rich spinel being followed by olivine, Type I (Ti-poor) phlogopite, and apatite, prior to the appearance of Type II (Ti-rich) phlogopite, richterite diopsidic clinopyroxene, and leucite (the latter two formed as resorption products of phlogopite), and, eventually, sanidine and Fe–Ti oxides. Cr-spinel and olivine phenocryst cores began crystallizing between ca. 1.0 and 2.0 GPa and temperatures of ca. 920–1050 °C. Type I micas probably began crystallizing at pressures of ca. 1.0–2.0 GPa, prior to their resorption and mantling by Type II phlogopite (at ca. 1.0–0.5 GPa). Apatite inclusions in the latter suggest their near-contemporaneous appearance with Type I phlogopite.

Melts forming K-rich phlogopite and richterite are considered to be a common metasomatic agent of the upper mantle. To generate partial melts with high concentrations of incompatible elements (light REE, Ba, Sr), the mantle source must have been previously enriched in these elements. Metasomatized peridotites are considered to be representative of enriched subcontinental lithosphere. However, the restriction of asthenospheric low velocities to the region beneath Isparta (Al-Lazki et al., 2004) suggest that the magmatic source region probably occupies a thermal boundary between the subcontinental lithosphere and shallow asthenosphere.

Compared to other lamproite magmatic products in the region, those from Bucak are distinguished by the assemblage of phlogopite (30–40%), leucite (25–30%), olivine (5–20%), clinopyroxene (5–10%), and sanidine (5%), with accessory richterite, apatite and Fe–Ti oxides although they are comparable to other silica-poor circum-Mediterranean ultrapotassic rocks with lamproitic affinity (e.g. from Jumilla, SE Spain and Macedonia and Yugoslavia, Eastern Europe). Estimates of magmatic fO_2 ratios (between or close to FMQ or Ni–NiO buffer conditions) suggest relatively oxidized crystallization conditions during their emplacement, consistent with those inferred for ultrapotassic magmas elsewhere.

Acknowledgements

This study was supported in part by Project No. 636 of the Scientific Exploration Unit of Suleyman Demirel University, Isparta, Turkey. We would like to thank Francois Rosseland who conducted whole-rock analyses in Lausanne University, Switzerland, and Drs. Roger Mitchell (Lakehead University, Ontario, Canada) and Orhan Karsli (Germany) for conducting the microprobe analyses.

References

Adams, G.E., Bishop, F.C., 1986. The olivine–clinopyroxene geobarometer: experimental results in the CaO–FeO–MgO–SiO_2 system. Contributions to Mineralogy and Petrology 94, 230–237.

Akal, C., Helvaci, C., 2002. K-richterite–olivine–phlogopite–diopside–sanidine lamproites from southern part of the Afyon volcanic province, western Turkey. 1st International Symposium of Earth Sciences and Engineering, Abstracts. ITU, Faculty of Mining, Istanbul, Turkey, p. 186.

Alici, P., Temel, A., Gourgaud, A., Kieffer, G., Gundogdu, M.N., 1998. Petrology and geochemistry of potassic rocks in the Golcuk area (Isparta, SW Turkey): genesis of enriched alkaline magmas. Journal of Volcanology and Geothermal Research 65, 1–24.

Al-Lazki, A.I., Sandvol, E., Seber, D., Barazangi, M., Turkelli, N., Mohammad, R., 2004. Pn tomographic imaging of mantle lid

velocity and anisotropy at the junction of the Arabian, Eurasian and African plates. Geophysical Journal International 158, 1024–1040.

Altherr, R., Meyer, H.P., Holl, A., Volker, F., Alibert, C., McCulloch, M.T., Majer, V., 2004. Geochemical and Sr–Nd–Pb isotopic characteristics of Late Cenozoic leucite lamproites from the East European Alpine belt (Macedonia and Yugoslavia). Contributions to Mineralogy and Petrology 147, 58–73.

Aoki, K., 1975. Origin of phlogopite and potassic richterite bearing peridotite xenoliths from South Africa. Contributions to Mineralogy and Petrology 53, 145–156.

Arai, S., 1994. Compositional variation of olivine–chromian spinel in Mg-rich magmas as a guide to their residual spinel peridotites. Journal of Volcanology and Geothermal Research 59, 279–293.

Arai, S., 1999. Origin of podiform chromites. Journal of Asian Earth Science 15, 2–3.

Arima, M., Edgar, A.D., 1983. High pressure experimental studies on a katungite and their bearing on the genesis of some potassium-rich magmas of the west branch of the African Rift. Journal of Petrology 24, 166–187.

Aydar, E., 1998. Early Miocene to Quaternary evolution of volcanism and the basin formation in western Anatolia: a review. Journal of Volcanology and Geothermal Research 85, 69–82.

Aydar, E., Gourgaud, A., Deniel, C., Lyberis, N., Gundogdu, N., 1995. Le volcanisme quaternaire de l'Anatolie centrale (Turquie): association de magmatism caco-alcalin en domaine de convergence. Canadian Journal of Earth Sciences 32, 1058–1069.

Aydar, E., Bayhan, H., Zimitoglu, O., 1996. Investigation of volcanological and petrological evolution of Afyon stratovolcano. Hacettepe University, Ankara, Bulletin of Earth Science Applied and Research Centre 18, 87–107.

Aydar, E., Bayhan, H., Gourgaud, A., 2003. The lamprophyres of Afyon stratovolcano, western Anatolia, Turkey: description and genesis. Comtes Rendus Geoscience 335, 279–288.

Ballhaus, C., Berry, R.F., Green, D.H., 1991. Oxygen fugacity controls in the earth's upper mantle. Nature 348, 437–440.

Basu, A.R., McGregor, I.O., 1975. Chromite spinels from ultramafic xenoliths. Geochimica et Cosmochimica Acta 39, 937–945.

Bayrak, M., Nalbant, S.S., 2001. Conductive crust imaged in Western Turkey by MT. Geophysical Research Letters 28, 3521–3524.

Bergman, S.C., 1987. Lamproites and other potassium-rich igneous rocks: a review of their occurrence, mineralogy and geochemistry. Fitton and Upton, q.v. , pp. 103–190.

Besang, C., Eckhardt, F.J., Harre, W., Kreuzer, H., Müller, P., 1977. Radiometrische Alterbestimmungen and Neogenen Eruptivgesteinen der Türkei. Geologisches Jahrbuch 25, 3–36.

Bindi, L., Cellai, D., Melluso, L., Conticelli, S., Mora, V., Menchetti, S., 1999. Crystal chemistry of clinopyroxene from alkaline undersaturated rocks of the Monte Vulture Volcano, Italy. Lithos 46, 259–274.

Bozkurt, E., Oberhansli, R., 2001. Menderes Massif (western Turkey): structural, metamorphic and magmatic evolution—a synthesis. International Journal of Earth Sciences 89, 679–708.

Brigatti, M.F., Gregnanin, A., 1987. Crystal chemistry of igneous rock biotites. Mineralogy and Petrology 37, 323–341.

Carmichael, I.S.E., 1967. The mineralogy and the petrology of the volcanic rocks from the Leucite Hills, Wyoming. Contributions to Mineralogy and Petrology 15, 24–66.

Carswell, D.A., 1975. Primary and secondary phlogopites and clinopyroxenes in garnet lherzolite xenoliths. Physics and Chemistry of Earth 9, 417–429.

Cellai, D., Conticelli, S., Menchetti, S., 1994. Crystal-chemistry of clinopyroxenes in Italian lamproites and kamafugites: implications on their genesis. Contributions to Mineralogy and Petrology 116, 301–315.

Cihan, M., Sarac, G., Oktay, G., 2003. Insights into biaxial extensional tectonics: an example from the Sandikli Graben, West Anatolia, Turkey. Geological Journal 38, 47–66.

Coban, H., Flower, M.F.J., in press. Late Pliocene lamproites from Bucak, Isparta (southwestern Turkey): implications for mantle 'wedge' evolution during Africa-Anatolian plate convergence. Journal of Asian Earth Science.

Collins, W.J., Beams, S.D., White, A.J.R., Chappell, B.W., 1982. Nature and origin of A-granites with particular reference to southeastern Australia. Contributions to Mineralogy and Petrology 80, 189–200.

Conticelli, S., 1998. The effect of crustal contamination on ultrapotassic magmas with lamproitic affinity: mineralogical, geochemical and isotope data from the Torre Alfina lavas and xenoliths, Central Italy. Chemical Geology 149, 51–81.

Conticelli, S., Peccerillo, 1992. Petrology and geochemistry of potassic and ultrapotassic volcanism in central Italy: petrogenesis and inferences on the evolution of the mantle sources. Lithos 28, 221–240.

Conticelli, S., Manetti, P., Menichetti, S., 1992. Petrology, chemistry, mineralogy, and Sr-isotopic data of Pliocenic orendites from South Tuscany: implications on their genesis and evolution. European Journal of Mineralogy 4, 1359–1375.

Conticelli, S., D'Antonio, M., Pinarelli, L., Civetta, L., 2002. Source contamination and mantle heterogeneity in the genesis of Italian potassic and ultrapotassic volcanic rocks: Sr–Nd–Pb isotope data from Roman Province and Southern Tuscany. Mineralogy and Petrology 74, 189–222.

Conticelli, S., Melluso, M., Perini, G., Avanzinelli, R., Borai, E., 2004. Petrologic, geochemical and isotopic characteristics of potassic and ultrapotassic magmatism in central–southern Italy: inferences on its genesis and on the nature of mantle source. Abstract LXXIII, Periodico di Mineralogia n. 1.

Cvetkovic', V., Prelevic', D., Downesb, H., Jovanovic', M., Vasellid, O., Pe cskaye, Z., 2004. Origin and geodynamic significance of Tertiary postcollisional basaltic magmatism in Serbia (central Balkan Peninsula). Lithos 73, 161–186.

Dawson, J.B., Smith, J.V., 1977. The MARID (Mica–Amphibole–Rutile–Ilmenite–Diopside) suite of xenoliths in kimberlite. Geochimica et Cosmochimica Acta 60, 423–437.

De Astis, G., Peccerillo, A., Pamela, D.K., Luigi, L.V., Tsai, W.W., 2000. Transition from calc-alkaline to potassium-rich magmatism in subduction environments: geochemical and Sr, Nd, Pb isotopic constraints from the island of vulcano (Aeolian arc). Contributions to Mineralogy and Petrology 139, 684–703.

Delaney, J.S., Smith, J.V., Carswell, D.A., Dawson, J.B., 1980. Chemistry of micas from kimberlites and xenoliths: II. Primary- and secondary-textured micas from peridotite xenoliths. Geochimica et Cosmochimica Acta 44, 857–872.

Doglioni, C., Agostini, S., Crespi, M., Innocenti, F., Manetti, P., Riguzzi, F., Savascin, Y., 2002. On the extension in western Anatolia and the Aegean sea. Journal of the Virtual Explore 8, 161–176.

Donaldson, C.H., 1976. An experimental investigation of olivine morphology. Contributions to Mineralogy and Petrology 57, 187–213.

Donaldson, C.H., 1979. An experimental investigation of the delay in nucleation of olivine in mafic magmas. Contributions to Mineralogy and Petrology 69, 21–32.

Droop, G.T.B., 1987. A general equation for estimating Fe^{3+} concentrations in ferromagnesian silicates and oxides from microprobe analyses, using stoichiometric criteria. Mineralogical Magazine 51, 431–435.

Duggan, M.B., 1988. Zirconium-rich sodic pyroxene in felsic volcanics from the Warrumbungle volcano, Central New South Wales, Australia. Mineralogical Magazine 52, 491–496.

Embey-Isztin, A., Downes, H., Kempton, P.D., Dobosi, G., Thirlwall, M., 2003. Lower crustal granulite xenoliths from the Pannonian Basin, Hungary: Part 1. Mineral chemistry, thermobarometry and petrology. Contributions to Mineralogy and Petrology 144, 652–670.

Ercan, T., Gunay, E., Bas, H., 1983. Denizli volkanitlerinin petrolojisi ve plaka tektonigi acisindan bolgesel yorumu. Bulletin of Geological Society of Turkey 26, 153–160.

Ercan, T., Satir, M., Kreuzer, H., Turkecan, A., Gunay, E., Cevikbas, A., Ates, M., Can, B., 1985. Bati Anadolu Senozoyik volkanitlerine ait yeni kimyasal, izotopik ve radyometrik verilerin yorumu. Bulletin of Geological Society of Turkey 28, 121–137 (in Turkish, with English Abstract).

Ercan, T., Satir, M., Sevin, D., Turkecan, A., 1996. Bati Anadoludaki Tersiyer ve Kuvaterner yasli volkanik kayaclarda yeni yapilan radyometrik yas olcumlerinin yorumu. Journal of MTA 119, 103–112.

Erlank, A.J., Waters, F.G., Hawkesworth, C.J., Haggerty, S.E., Allsopp, H., Rickard, R.S., Menzies, M.A., 1987. Evidence for mantle metasomatism in peridotite nodules from the Kimberley pipes, South Africa. In: Menzies, M.A., Hawkesworth, C.J. (Eds.), Mantle Metasomatism. Academic Press Geology Series, pp. 221–312.

Ferguson, A.K., 1977. The natural occurrence of aegirine–neptunite solid solution. Contributions to Mineralogy and Petrology 60, 247–253.

Foley, S.F., 1989a. The genesis of lamproitic magmas in a reduced fluorine-rich mantle. In: Ross, J. (Ed.), Kimberlite and Related Rocks: I. Their Composition, Occurrence, Origin and EmplacementSpecial Publication. Geological Society of Australia, vol. 14, pp. 616–631.

Foley, S.F., 1989b. Experimental constraints on phlogopite chemistry in lamproites: 1. Effect of water activity and oxygen fugacity. European Journal of Mineralogy 1, 411–426.

Foley, S.F., 1990. Experimental constraints on phlogopite chemistry in lamproites: 2. Effects of pressure–temperature variations. European Journal of Mineralogy 2, 327–341.

Foley, S.F., 1991. High pressure stability of the fluor- and hydroxy-end members of pargasite and K-richterite. Geochimica et Cosmochimica Acta 55, 2689–2694.

Foley, S.F., 1992a. Petrological characterization of the source components of potassic magmas: geochemical and experimental constraints. Lithos 28, 187–204.

Foley, S.F., 1992b. Vein-plus-wall-rock melting mechanisms in the lithosphere and the origin of potassic alkaline magmas. Lithos 28, 435–453.

Foley, S.F., 1993. An experimental study of olivine lamproite: first results from the diamond stability field. Geochimica et Cosmochimica Acta 57, 483–489.

Foley, S.F., Taylor, W.R., Green, D.H., 1986a. The effect of fluorine on phase relationship in the system $KalSiO_4$–Mg_2SiO_4–SiO_2 at 28 kbar and the solution mechanism of fluorine in silicate melts. Contributions to Mineralogy and Petrology 93, 46–55.

Foley, S.F., Taylor, W.R., Green, D.H., 1986b. The role of fluorine and oxygen fugacity in the genesis of the ultrapotassic rocks. Contributions to Mineralogy and Petrology 94, 183–192.

Foley, S.F., Venturelli, G., Green, D.H., Toscani, L., 1987. The ultrapotassic rocks: characteristics, classification and constraints for petrogenetic models. Earth Science Reviews 24, 81–134.

Forbes, W.C., Flower, M.F.J., 1974. Phase relations of titan–phlogopite, $K_2Mg_4TiAl_2Si_24(OH)_2$: a refractory phase in the upper mantle? Earth and Planetary Science Letters 22, 60–66.

Francalanci, L., Civetta, L., Innocenti, F., Manetti, P., 1990. Tertiary–Quaternary alkaline magmatism of the Aegean-Western Anatolian area: a petrological study in the light of new geochemical and isotopic data. Int. Earth Sciences Cong. on Aegean Regions (IESCA), DEU, Izmir, Turkey, pp. 385–396.

Francalanci, L., Innocenti, F., Manetti, P., Savascin, M.Y., 2000. Neogene alkaline volcanism of the Afyon-Isparta area, Turkey: petrogenesis and geodynamic implications. Mineralogy and Petrology 70, 285–312.

Glover, C.P., Robertson, A.H.F., 1998a. Role of regional extension and uplift in the Plio-Pleistocene evolution of the Aksu Basin, SW Turkey. Journal of Geological Society of London 155, 365–387.

Glover, C.P., Robertson, A.H.F., 1998b. Neotectonic intersection of the Aegean and Cyprus tectonic arcs: extensional and strike-slip faulting in the Isparta Angle, SW Turkey. Tectonophysics 298, 103–132.

Green, T.H., 1995. Significance of Nb/Ta as an indicator of geochemical processes in the crust–mantle system. Chemical Geology 120, 347–359.

Green, D.H., Falloon, T.J., Eggins, S.M., Yaxley, G.M., 2001. Primary magmas and mantle temperatures. European Journal of Mineralogy 13, 437–451.

Gregoire, M., Bell, D.R., Le Roex, A.P., 2002. Trace element geochemistry of phlogopite-rich mafic mantle xenoliths: their classification and their relationship to phlogopite-bearing peridotites and kimberlites revisited. Contributions to Mineralogy and Petrology 142, 603–625.

Grove, T.L., Juster, T.C., 1989. Experimental investigations of low-Ca pyroxene stability and olivine–pyroxene–liquid equilibria at 1 atm in natural basaltic and andesitic liquids. Contributions to Mineralogy and Petrology 103, 287–305.

Gulec, N., 1991. Crust–mantle interaction in Western Turkey: implication from Sr and Nd isotope geochemistry of the Tertiary and Quaternary volcanics. Geological Magazine 128, 417–435.

Gupta, A.K., Green, D.H., 1988. The liquidus surface of the system Forsterite–Kalsilite–Quartz at 28 kbar under dry conditions, in presence of H_2O and CO_2. Mineralogy and Petrology 39, 163–174.

Gursoy, H., Piper, J.D.A., Tatar, O., 2003. Neotectonic deformation in the western sector of tectonic escape in Anatolia: palaeomagnetic study of the Afyon region, Central Turkey. Tectonophysics 374, 57–59.

Haggerty, S.E., Agnes, T.F., Burt, D.M., 1994. Apatite, phosphorous and titanium in eclogite garnet from the upper mantle. Geophysical Research Letters 21, 1699–1702.

Hancer, M., Karaman, E., 2001. Tectonic features of Bucak and its surrounding (southern Isparta). 4th Int. Symp. on Eastern Mediterranean Geology, Isparta, Turkey, pp. 33–43.

Harte, B., Winterburn, P.A., Gurney, J.J., 1987. Metasomatic and enrichment phenomena in garnet peridotite facies mantle xenoliths from the Matsuko kimberlite pipe, lesotho. In: Menzies, M.A., Hawkesworth, C.J. (Eds.), Mantle Metasomatism. Academic Press Geology Series, pp. 145–220.

Hawthorne, F.C., 1983. The crystal chemistry of amphiboles. Canadian Mineralogist 21, 173–480.

Ilkisik, O.M., 1997. Regional heat flow in western Anatolia using silica temperature estimates from thermal springs. Tectonophysics 244, 175–184.

Ionov, D.A., Hofmann, A.W., 1995. Nb–Ta-rich amphiboles and micas: implications for subduction-related metasomatic trace element fractionations. Earth and Planetary Science Letters 131, 341–356.

Jaques, A.L., Green, D.H., 1980. Anhydrous melting of peridotite at 0–15 kb pressure and the genesis of tholeiitic basalts. Contributions to Mineralogy and Petrology 73, 287–310.

Jaques, A.L., Lewis, J.D., Smith, C.B., 1986. The kimberlites and lamproites of Western Australia. Geological Survey of Western Australia Bulletin 132, 268.

Kamenetsky, V.S., Crawford, A.J., Meffre, S., 2001. Factors controlling chemistry of magmatic spinel: an empirical study of associated olivine, Cr-spinel and melt inclusions from primitive rocks. Journal of Petrology 42, 571–655.

Keller, J., 1983. Potassic lavas in the orogenic volcanism of the Mediterranean area. Journal of Volcanology and Geothermal Research 18, 321–335.

Kempton, P.D., Downes, H., Sharkov, E.V., Vetrin, V.R., Ionov, D.A., Carswell, D.A., Beard, A., 1995. Petrology and geochemistry of xenoliths from the Northern Baltic shield: evidence for partial melting and metasomatism in the lower crust beneath an Archean terrane. Lithos 36, 157–184.

Kocyigit, A., 1984. Intra-plate neotectonic development in South-western Turkey and adjacent areas. Bulletin of Geological Society of Turkey 27, 1–16.

Kocyigit, A., Ünay, E., Sarac, G., 2002. Episodic graben formation and extensional neotectonic regime in west central Anatolia and the Isparta Angle: a case study in the Akşehir-Afyon graben, Turkey. In: Bozkurt, E., Winchester, J.A., Piper, J.D.A. (Eds.), Tectonics and Magmatism in Turkey and the Surrounding Area. Geological Society, London, Special Publication, vol. 173, pp. 405–421.

Kogarko, L.N., Lazutkina, L.N., 1988. Zirconium in silicate liquids and magmas. Geochemical International 26, 47–56.

Kohler, T.P., Brey, G.P., 1990. Calcium exchange between olivine and clinopyroxene calibrated as a geothermobarometer for natural peridotites from 2 to 60 kb with applications. Geochimica et Cosmochimica Acta 54, 2375–2388.

Konzet, J., 1997. Phase relations and chemistry of Ti-rich K-richterite-bearing mantle assemblages: an experimental study to 8.0 GPa in a Ti-KNCMASH system. Contributions to Mineralogy and Petrology 128, 385–404.

Lefevre, C., Bellon, H., Poisson, A., 1983. Presence de leucitites dans le volcanism Pliocene de la region d'Isparta (Taurides occidentales, Turquie). Comptes Rendus de l'Academie des Sciences 297, 367–372.

Le Maitre, R.W., Streckeisen, A., Zanettin, B., Le Bas, M.J., Bonin, B., Bateman, P., Bellieni, G., Dudek, A., Efremova, S., Keller, J., Lameyre, J., Sabine, P.A., Schmid, R., Sørensen, H., Woolley, A. R., 2002. Igneous rocks: a classification and glossary of terms. Recommendations of the International Union of Geological Sciences Subcommission on the Systematics of Igneous Rocks. Cambridge University Press, p. 236.

Luth, W.C., 1967. Studies in the system $KalSiO_4$–Mg_2SiO_4–SiO_2–H_2O: I. Inferred phase relations and petrologic application. Journal of Petrology 8, 372–416.

Mitchell, R.H., 1981. Titaniferrous phlogopites from the leucite lamproites of the West Kimberley area, Western Australia. Contributions to Mineralogy and Petrology 76, 243–251.

Mitchell, R.H., 1985. A review of the mineralogy of lamproites. Transactions of Geological Society of South Africa 88, 411–437.

Mitchell, R.H., Bergman, S.C., 1991. Petrology of Lamproites. Plenum Press, Newyork. 447 pp.

Murphy, D.T., Collerson, K.D., Kamber, B.S., 2002. Lamproites from Gaussberg, Antarctica: possible transition zone melts of Archean subducted sediments. Journal of Petrology 43, 981–1001.

Nash, W.P., Wilkinson, J.F.G., 1970. Shonkin Sag laccolith, Montana. 1. Mafic minerals and estimates of temperature, pressure, oxygen fugacity and silica activity. Contributions to Mineralogy and Petrology 25, 241–269.

Nasir, S., 1996. Peridot: software package for the estimation of pressure–temperature–oxygen fugacity of upper mantle and lower crustal mineral assemblages. Computers and Geosciences 22, 589–591.

Nell, J., Wood, B.J., 1991. High-temperature electrical measurements and thermodynamic properties of Fe_3O_4–$FeCr_2O_4$–$MgCr_2O_4$–$FeAl_2O_4$ spinels. American Mineralogist 76, 405–426.

Nelson, D.R., McCulloch, M.T., Sun, S.S., 1986. The origins of ultrapotassic rocks as inferred from Sr, Nd and Pb isotopes. Geochimica et Cosmochimica Acta 50, 231–245.

Niida, K., Green, D., 1999. Stability and chemical composition of pargasitic amphibole in MORB pyrolite under upper mantle conditions. Contributions to Mineralogy and Petrology 135, 18–40.

Nimis, P., 1995. A clinopyroxene geobarometer for basaltic systems based on crystal-structure modeling. Contributions to Mineralogy and Petrology 121, 115–125.

Nimis, P., 1998. Evaluation of diamond potential from the composition of peridotitic chromian diopside. European Journal of Mineralogy 10, 505–519.

O'Neill, H.St., 1981. The transition between spinel lherzolite and garnet lherzolite, and its use as a geobarometer. European Journal of Mineralogy 77, 185–194.

O'Neill, H.S.C., Wall, V.J., 1987. The olivine–Orthopyroxene–Spinel oxygen geobarometer, the nickel precipitation curve, and the oxygen fugacity of the Earth's Upper mantle. Journal of Petrology 28, 1169–1191.

Papazachos, B.C., Papaioannou, Ch.A., 1999. Lithospheric boundaries and plate motions in the Cyprus area. Tectonophysics 308, 193–204.

Paton, S.M., 1992. The relationship between extension and volcanism in western Turkey, the Aegean Sea and central Greece. PhD thesis, Cambridge University.

Pe, G.G., Gledhill, C., 1975. Strontium isotope ratios in volcanic rocks from the south-eastern part of the Hellenic arc. Lithos 8, 209–214.

Peccerillo, A., 1999. Multiple mantle metasomatism in central southern Italy: geochemical effects, timing and geodynamic implications. Geology 27, 315–318.

Peccerillo, A., Poli, G., Serri, G., 1988. Petrogenesis of orenditic and kamafugitic rocks from central Italy. Canadian Mineralogist 26, 45–65.

Perini, G., Conticelli, S., 2002. Crystallization conditions of leucite-bearing magmas and their implications on the magmatological evolution of ultrapotassic magmas: the Vico volcano, Central Italy. Mineralogy and Petrology 74, 253–276.

Perini, G., Conticelli, S., Francalanci, L., Davidson, J.P., 2000. The relationship between potassic and calc-alkaline post-orogenic magmatism at Vico volcano, central Italy. Journal of Volcanology and Geothermal Research 95, 247–272.

Ramsay, R.R., 1992. Geochemistry of diamond indicator minerals. PhD Thesis, University of Western Australia, Perth.

Rickers, K., Raith, M., Dasgupta, S., 2001. Multistage reaction textures in xenolithic high-Mg–Al granulites at Anakapalle, Eastern Ghats Belt, India: examples of contact polymetamorphism and infiltration-driven metasomatism. Journal of Metamorphic Geology 19, 563–582.

Righter, K., Carmichael, S.E.I., 1996. Phase equilibria of phlogopite lamprophyres from western Mexico: biotite–liquid equilibria and *P–T* estimates for biotite-bearing igneous rocks. Contributions to Mineralogy and Petrology 123, 1–21.

Rizzo, G., Piluso, E., Morten, L., 2001. Phlogopite from the Serre ultramafic rocks, Central Calabria, Southern Italy. European Journal of Mineralogy 13, 1139–1151.

Robert, U., Foden, J., Varne, R., 1992. The Dodecanese Province, SE Aegean: a model for tectonic control on potassic magmatism. Lithos 28, 241–260.

Robertson, A.H.F., 2000. Mesozoic–Tertiary tectonic-sedimentary evolution of a south Tethyan oceanic basin and its margins in southern Turkey. In: Bozkurt, E., Wýnchester, J.A., Pıper, J.D.A. (Eds.), Geological Society of London, Special Publications. Tectonics and Magmatism in Turkey and the Surrounding Area, pp. 97–138.

Robertson, 2002. Overview of the genesis and emplacement of Mesozoic ophiolites in the Eastern Mediterranean Tethyan region. Lithos 65, 1–67.

Roder, P.L., 1974. Activity of iron and olivine solubility in basaltic liquids. Earth and Planetary Science Letters 23, 397–410.

Roder, P.L., Emslie, R.F., 1970. Olivine liquid equilibrium. Contributions to Mineralogy and Petrology 29, 275–289.

Saunders, P., Priestley, K., Taymaz, T., 1998. Variations in the crustal structure beneath western Turkey. Geophysical Journal International 134, 373–389.

Savascin, Y., Gulec, N., 1990. Relationship between magmatic and tectonic activities in Western Turkey. İzmir, Proceedings of International Earth Science Congress of Aegean Region 1, pp. 300–314.

Savascin, Y., Oyman, T., 1998. Tectono-magmatic evolution of Alkaline Volcanics at the Kirka-Afyon-Isparta Structural Trend, SW Turkey. Turkish Journal of Earth Sciences 7, 201–214.

Simkin, T., Smith, J.V., 1970. Minor-element distribution in olivine. Journal of Geology 78, 304–325.

Smith, J.V., Herving, R.L., Ackermand, D., Dawson, J.B., 1979. K, Rb and Ba in micas from kimberlite and peridotitic xenoliths and implications for origin of basaltic rocks. In: Boyd, F.R., Meyer, H. O.A. (Eds.), Kimberlites, Diatrems, and Diamonds: Their Geology, Petrology and Geochemistry. American Geophysical Union, vol. 1, pp. 241–251.

Spencer, K.J., Lindsley, D.H., 1981. A solution model for coexisting iron–titanium oxides. American Mineralogist 66, 1189–1201.

Stephenson, D., Upton, B.G.J., 1982. Ferromagnesian silicates in a differential alkaline complex: Kungnat Fjeld, South Greenland. Mineralogical Magazine 46, 283–300.

Sudo, A., Tatsumi, Y., 1990. Phlogopite and K-amphibole in the upper mantle: implication for magma genesis in subduction zones. Geophysical Research Letters 13, 717–720.

Sun, S.S., McDonough, W.F., 1989. Chemical and isotopic systematics of oceanic basalts: implications of mantle composition and processes. In: Saunders, A.D., Norry, M.J. (Eds.), Magmatism in the Ocean Basins. Geological Society of London, Special Publication, vol. 42, pp. 313–345.

Thompson, R.N., 1974. Some high-pressure pyroxenes. Mineralogical Magazine 39, 768–787.

Tieopolo, M., Vannucci, R., Oberti, R., Foley, S., Bottazzi, P., Zanetti, A., 2000. Nb and Ta incorporation and fractionation in titanian pargasite and kaersutite: crystal-chemical constraints and implications for natural systems. Earth and Planetary Science Letters 176, 185–201.

Turner, S.P., Platt, J.P., George, R.M.M., Kelley, S.P., Pearson, D.G., Nowell, G.M., 1999. Magmatism associated with orogenic collapse of the Betic-Alboran domain, SE Spain. Journal of Petrology 10, 1011–1036.

Ulmer, P., 1989. The dependence of the Fe+2-Mg cation-partitioning between olivine and basaltic liquid on pressure, temperature and composition. An experimental study to 30 kbars. Contributions to Mineralogy and Petrology 101, 261–273.

Upton, B.G.J., Aspen, P., Hinton, R.W., 2001. Pyroxenite and granulite xenoliths from beneath the Scottish Northern Highlands Terrane: evidence for lower crust/upper-mantle relationships. Contributions to Mineralogy and Petrology 142, 178–197.

Van Achterbergh, E., Griffin, W.L., Stiefenhofer, J., 2001. Metasomatism in mantle xenoliths from the Letlhakane kimberlites: estimation of element fluxes. Contributions to Mineralogy and Petrology 141, 397–414.

Vaughan, A.P.M., Scarrow, J.H., 2003. K-rich mantle metasomatism control of localization and initiation of lithospheric strike-slip faulting. Terra Nova 15, 163–169.

Venturelli, G., Capedri, S., Di Battistini, G., Crawford, A.J., Kogarko, L.N., Celestini, S., 1984a. The ultrapotassic rocks from southeastern Spain. Lithos 17, 37–54.

Venturelli, G., Thorpe, R.S., Dal Piaz, G.V., Del Moro, A., Potts, P.J., 1984b. Petrogenesis of calc-alkaline, shoshonitic and associated ultrapotassic Oligocene volcanic rocks from the Northwestern Alps, Italy. Contributions to Mineralogy and Petrology 86, 209–220.

Venturelli, G., Salvioli-Maniani, E., Foley, S.F., Capedri, S., Crawford, AJ., 1988. Petrogenesis and conditions of crystallization of Spanish lamproitic rocks. Canadian Mineralogist 26, 67–80.

Venturelli, G., Capedri, S., Barbieri, M., Toscani, L., Salvioli Mariani, E., Zerbi, M., 1991. The Jumilla lamproite revisited: a petrological oddity. European Journal of Mineralogy 3, 123–145.

Wagner, C., Velde, D., 1986. The mineralogy of K-richterite-bearing lamproites. American Mineralogist 71, 17–37.

Wagner, C., Deloule, E., Mokhtari, A., 1996. Richterite-bearing peridotites and MARID-type inclusions in lavas from North Eastern Morocco: mineralogy and D/H isotopic studies. Contributions to Mineralogy and Petrology 124, 406–421.

Watson, E.B., 1979. Zircon saturation in felsic liquids: experimental results and application to trace element geochemistry. Contributions to Mineralogy and Petrology 70, 407–419.

Web, S.A.C., Wood, B.S., 1986. Spinel–pyroxene–garnet relationships and their dependence on Cr/Al ratio. Contributions to Mineralogy and Petrology 92, 471–480.

Wendlandt, R.F., Eggler, D.H., 1980. The origin of potassic magmas: 2. Stability of phlogopite in natural spinel lherzolite and in the system $KAlSiO_4$–MgO–SiO_2–H_2O–CO_2 to 30 kb. American Journal of Science 280, 421–458.

Wulff-Pedersen, E., Neumann, E.R., Jensen, B.B., 1996. The upper mantle under La Palma, Canary Islands: formation of Si–K–Na-rich melt and its importance as a metasomatic agent. Contributions to Mineralogy and Petrology 125, 113–139.

Wulff-Pedersen, E., Neumann, E.R., Vannucci, R., Bottazzi, P., Ottolini, L., 1999. Silicic melts produced by reaction between

peridotite and infiltrating basaltic melts: ion probe data on glasses and minerals in veined xenoliths from La Palma, Canary Islands. Contributions to Mineralogy and Petrology 137, 59–82.

Yagmurlu, F., Savascin, M.Y., Ergun, M., 1997. Relation of alkaline volcanism and active tectonism within the evolution of Isparta Angle, SW Turkey. Journal of Geology 105, 717–728.

Zanetti, A., Vannucci, R., Bottazzi, P., Oberti, R., Ottolini, L., 1996. Infiltration metasomatism at Lherz as monitored by systematic ion/probe investigations close to a hornblendite vein. Chemical Geology 134, 113–133.

Zanetti, A., Mazzucchelli, M., Rivalenti, G., Vannucci, R., 1999. The Finero–phlogopite–peridotite massif: an example of subduction-related metasomatism. Contributions to Mineralogy and Petrology 134, 107–122.

Zhang, M., Suddaby, P., O'Reilly, S.Y., Norman, M., Qiu, J., 2000. Nature of the lithospheric mantle beneath the eastern part of the Central Asian fold belt: mantle xenolith evidence. Tectonophysics 328, 131–156.